

Document downloaded from:

<http://hdl.handle.net/10251/63903>

This paper must be cited as:

Escorihuela Fuentes, J.; González Martínez, M.Á.; López-Paz, J.L.; Puchades, R.; Angel Maquieira Catala (2015). Dual-Polarization Interferometry: A Novel Technique To Light up the Nanomolecular World. *Chemical Reviews*. 115(1):265-294. doi:10.1021/cr5002063.



The final publication is available at

<https://dx.doi.org/10.1021/cr5002063>

Copyright American Chemical Society

#### Additional Information

This document is the Accepted Manuscript version of a Published Work that appeared in final form in

*Chemical Reviews*, copyright © American Chemical Society after peer review and technical editing by the publisher.

To access the final edited and published work see <http://pubs.acs.org/doi/abs/10.1021/cr5002063>.

# Dual Polarization Interferometry. A Novel Technique to Light up the Nanomolecular World

Jorge Escorihuela<sup>1</sup>, Miguel Ángel González-Martínez<sup>1</sup>, José Luis López-Paz<sup>1</sup>, Rosa Puchades<sup>1</sup>, Ángel Maquieira<sup>1</sup> and David Gimenez-Romero<sup>2\*</sup>

<sup>1</sup>Departament of Chemistry, Institute of Molecular Recognition and Technological Development, Universitat Politècnica de València, Camino de Vera s/n, 46022 València, Spain

<sup>2</sup> Physical Chemistry Department, Faculty of Chemistry, Universitat de València, Avda. Dr. Moliner 50, 46100 Burjassot, València, Spain.

**Keywords:** Dual polarization interferometry, Biophysics, Biosensor, Protein, DNA, Conformational dynamics.

## Contents

1. Introduction
2. General Principles
  - 2.1. Assumptions and more complex models
    - 2.1.1. Anisotropy
3. Measurement
4. Comparison and combination with other techniques
5. Bioreceptor immobilization
  - 5.1. General remarks
  - 5.2. Protein attachment
    - 5.2.1. Physical adsorption
    - 5.2.2. Biochemical affinity
    - 5.2.3. Covalent immobilization
  - 5.3. DNA attachment
    - 5.3.1. Physical adsorption
    - 5.3.2. Avidin-biotin interaction
    - 5.3.3. Covalent immobilization
6. Applications
  - 6.1. Protein Studies
    - 6.1.1. Characterization and conformational changes
    - 6.1.2. Crystallization monitoring
    - 6.1.3. Adsorption
    - 6.1.4. Interactions
      - 6.1.4.1. Antibody
      - 6.1.4.2. Protein ligand
      - 6.1.4.3. Non-protein ligand
  - 6.2. DNA Studies
    - 6.2.1. Immobilization and hybridization events
    - 6.2.2. Interactions with small molecules
  - 6.3. Lipid and membrane studies
  - 6.4. Polymer and polyelectrolyte studies
    - 6.4.1. Single layer adsorption
    - 6.4.2. Layer-by-Layer deposition
    - 6.4.3. Polymer interactions
  - 6.5. Surface Characterization
  - 6.6. Other Applications

7. Future remarks
8. Conclusions
9. Acknowledgments
10. References
11. Biographies

## 1. Introduction

The challenging lecture given in 1959 by physicist and Nobel Prize awarded R. P. Feynman: “There's plenty of room at the bottom” is considered to be the starting point for nanotechnology. With this peculiar title, Feynman encouraged researchers to explore beyond the atomic level and predicted exciting new phenomena that might revolutionize science and technology. Among these pioneering researchers are Eric Betzig, Stefan W. Hell and William E. Moerner, who have been awarded with the Nobel Prize in Chemistry 2014 for developing the super-resolved fluorescence microscopy. However, it is important to remark that the exploration of this amazing nanomolecular world began in the early 1980s with the invention of the scanning tunneling<sup>1</sup> and the atomic force microscopes<sup>2</sup> (Figure 1).

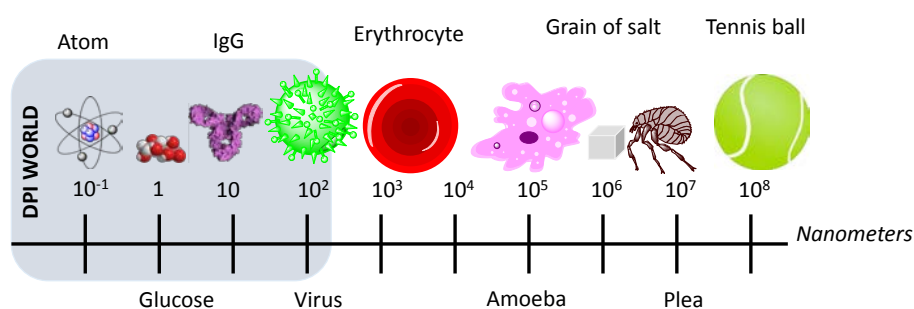


**Figure 1.** Measurement scales.

The study and manipulation of interactions of nanometric dimensions could begin as soon as measuring tools became more efficient. The last decades have witnessed the development of techniques able to obtain information at the sub-molecular level, and their applications especially on the biomedical field. As an example, the stimulating labor of studying the role of conformational dynamics in reaction mechanisms has resulted in

numerous advances in life sciences.<sup>3</sup> In this regard, the precise knowledge about molecular interactions and their effects on protein function has greatly aided the discovery of new targets in medical chemistry.

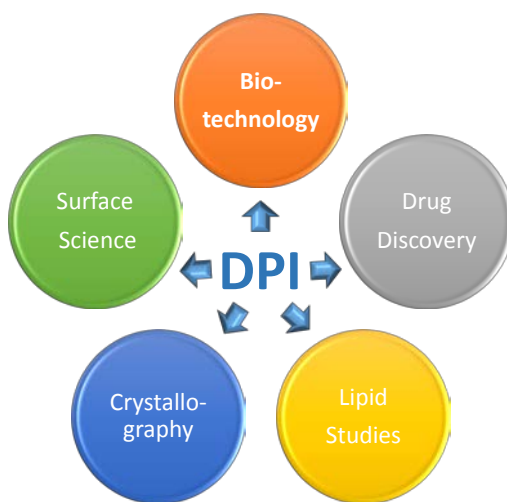


**Figure 2.** General scheme of different DPI applications.

The role of the structure in the protein behavior is a fundamental step in the utilization, characterization and understanding of numerous biological processes. Consequently, highly advanced functional and structural measurement tools have been developed over the last decades.<sup>4</sup> Particularly, nuclear magnetic resonance (NMR), X-ray crystallography and neutron reflectivity (NR) provide structural measurements, whereas tools such as microcalorimetry or surface plasmon resonance (SPR) provide functional data. Furthermore, the more recent approach based on Dual Polarization Interferometry (DPI), is allowing the molecular interactions to be quantitatively measured at nanometric dimensions.

DPI is currently one of the most powerful label-free biosensing techniques in heterogeneous format to record real-time data of conformational dynamics, which is efficiently employed in different applications, such as bionanotechnology, surface science,

and crystallography or drug discovery (Figure 2). Their measurements can provide information about the connection between the biomolecule function and its structural changes. This technique is, to our knowledge, the most well-built and well-thought through such waveguide sensor. It has its weaknesses, e.g. the necessity of using a relatively long sensor element, but the information it delivers is the interaction of two polarization modes of the propagating light with a molecular film at the top of the waveguide with which it interacts through the evanescent field. It is well known that the use of an interferometric readout and a long waveguide makes the measurements very stable and more accurate than those of the competitor techniques. Accordingly, DPI can be described as a *molecular ruler* whose quantitative values can be correlated directly with those from other usual techniques, such as NMR, X-ray crystallography and NR, providing higher sensitivity and accuracy than the classical acoustic and optical biosensors.

In 1996, Dr Neville Freeman conceived of the idea behind DPI as a robust and reproducible biosensing technology and, together with Dr Graham Cross, developed the concept and filed the original patent.<sup>5,6</sup> This novel technique has gained popularity among the scientific community in the last decade and the number of publications dealing with this technique has increased considerably since the initial report in 2003.<sup>7</sup> In this review, DPI is compared with other techniques, and its theoretical basis and applications are outlined. The fundamentals are specified together with strategies for chip functionalization and applications of the aforementioned technology in a wide variety of research areas. All this gives a unique chance to learn from this sensing technique, which may be an essential reference to facilitate the work of future users.

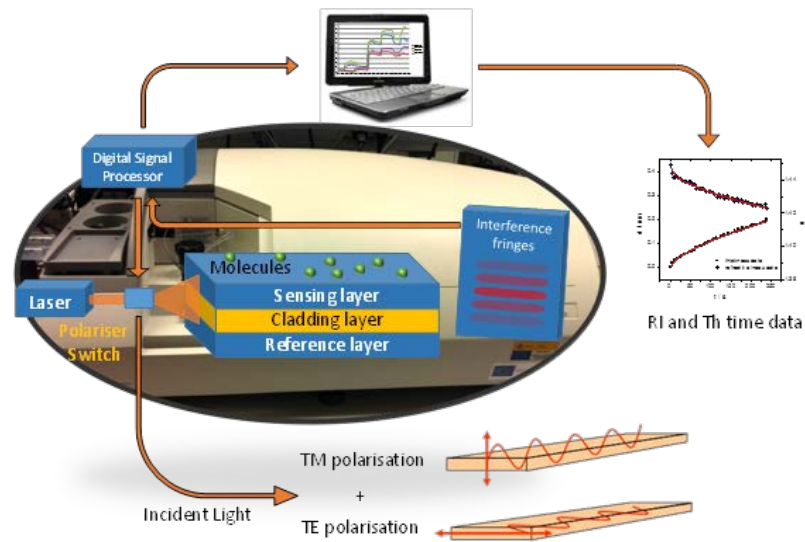


**Figure 3.** Schematic representation of a typical DPI sensor.

## 2. General Principles

Interferometry belongs to a family of techniques in which waves, usually electromagnetic, are superimposed in order to gain information about them.<sup>8</sup> Optical waveguide interferometers are based on the detection of the phase change,  $\Delta\phi$ , underwent by a light wave along the sensing path. This change is due to alterations in sample refractive index and layer thickness on the waveguide. Nevertheless, Maxwell's equations allow the effective medium refractive index to be only estimated, because there is not enough information to calculate simultaneously both parameters from a single interference pattern.<sup>9</sup> Fortunately, DPI allows both parameters to be measured almost simultaneously, because it measures two different interference fringe patterns. These patterns can be mathematically resolved into refractive index and thickness values and hence, the final outcome is a measurement in real-time of both parameters.<sup>10</sup>

Although the complexity of the optical technology generally requires the use of sophisticated equipment, DPI employs a simplified slab waveguide interferometer, where the reference layer is located under the sensing waveguide.<sup>5,11</sup> Slab waveguides are structures with a planar geometry, which guide light in only one transverse direction as lateral modes become effectively infinite. An important advantage of this configuration is the absence of scattering between transverse and lateral modes.

In a DPI instrument (Figure 3), the laser light broadly illuminates the end face of the two stacked planar waveguides without the usual need for focusing as would be the case for end-firing into a channel waveguide or fibre. A small portion of the light is coupled into each of the two waveguides; whilst one acts as a sensing waveguide having a surface exposed to the solution, the second one is used as a reference. As a consequence, on emerging from the waveguide structure, a two-dimensional interference pattern from light passing along both waveguides can be obtained in the far field.<sup>5</sup> The input power coupling efficiency is about -26 dB for each waveguide.<sup>12</sup> Furthermore, the design of the waveguide stack allows transverse-magnetic (TM) and transverse-electric (TE)-polarizations passing along the sensing and reference waveguides, which enables the measurement of two optical phase changes. The polarization can be switched rapidly (on a 2 ms cycle), allowing instantaneous measurements of molecular processes occurring on the sensing waveguide.

Light with an electric field vector perpendicular to the direction of the waveguide is commonly known as transverse-magnetic wave, whereas the parallel component is named transverse-electric wave. In both, the laser light, which is produced by a traceable and stable Helium-Neon laser ( $\lambda = 632.8$  nm and 20 mW), possesses the same frequency

and is confined within the waveguide structure. However, one important difference is found in the distribution of the light within the waveguide and in the evanescent field magnitude and in the profile (the shape of the decay of the beam intensity vs distance to the surface), as they differ in both polarization modes (Figure 3). Particularly, the TE mode profile is more closely confined to the surface of the waveguide than the TM mode profile and therefore, it is more influenced by changes in refractive index taking place on the surface than the TM. Consequently, the occupation density of the sensing layer is broadly proportional to the TE mode fringe phase changes ( $\Delta\phi_{TE}$ , resolution  $< 0.1$  pg/mm<sup>2</sup>), whereas the effective refractive index of this layer (resolution  $\approx 10^{-7}$  units) is proportional to the retardation,  $\Delta\phi_{TE}/\Delta\phi_{TM}$ , irrespective of their magnitudes.

The input light polarization is changed between TE and TM modes by a liquid-crystal wave plate at 500 Hz. The output two-dimensional interference patterns formed from both modes allow, by Fourier transformation, the accumulated real-time mode fringe phase changes,  $\Delta\phi_{TE}$  and  $\Delta\phi_{TM}$ , to be measured during the deposition of the layer (Figure 4).<sup>5</sup> Typically, solutions to Maxwell's equations for a one-dimensional multilayer dielectric continuum electrodynamic model (known as "Resolver") are calculated from these phase changes, so estimating the layer thickness and the effective medium refractive index.<sup>7,13,14</sup> By assuming that a surface layer is formed, two ranges of values (blended values of layer refractive index and thickness) that satisfy the observed TM and TE modes fringes movement can be obtained (Figure 5). In both TE and TM solution ranges, there is a single point of intersection, where the two series of computed layer thickness and refractive index values obtained for both polarization modes are overlaid. This point corresponds to the layer conditions on the waveguide surface at each time  $t$ . The described

process is used to obtain layer thickness and refractive index measurements throughout the experiment.

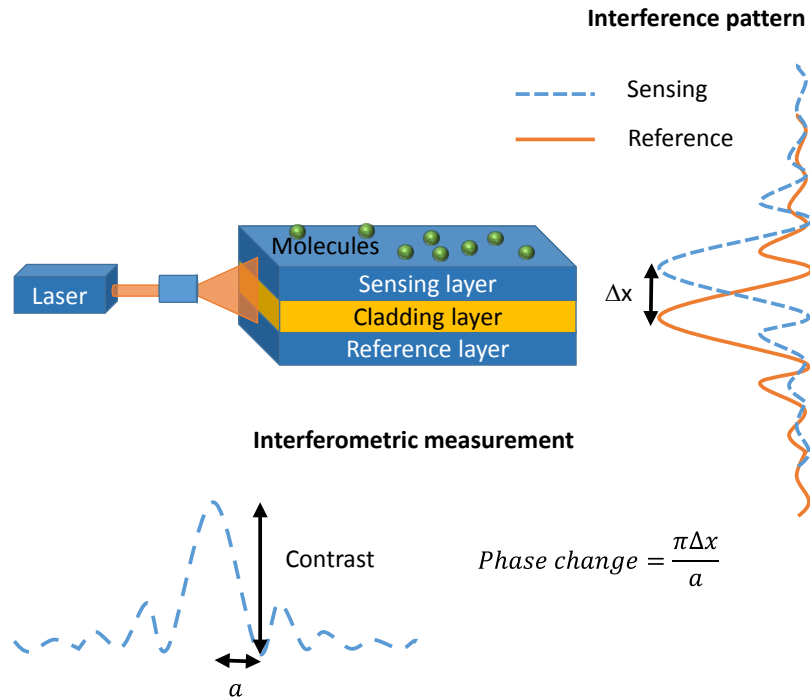


**Figure 4.** Key features of the detected fringe patterns.

Another key feature of the detected fringe patterns is the fringe contrast; that is, the difference of intensity between the peak apex and the peak valley within the fringes (Figure 4).<sup>15</sup> This value is a measurement of the difference in the light amount that passes through both waveguides, and consequently, it is influenced by any losses, i.e. absorption or scattering, that take place on the detection surface. Hence, this information allows structural characteristics of the monitored layer to be inferred, e.g. stochastic versus nucleated packing. Contrast loss can be an alternative method to calculate mass for optically absorbing molecules. Losses from the waveguide structure are observed during crystallization processes. However, they are of much smaller magnitude than those produced as a result of precipitation, aggregation and other non-ordered solid-state

phases, which allows these states to be distinguished. Alternatively, the change in contrast can be associated with the amount of light absorbing material on or above the chip.

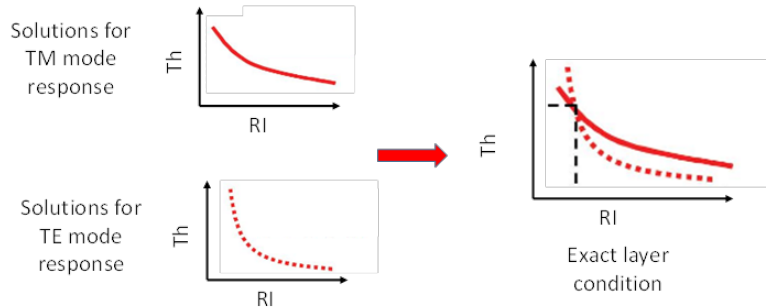


**Figure 5.** Refractive index and thickness estimation for the TE and TM modes fringes movement.

## 2.1. Assumptions and more complex models

Due to the potential applications of DPI, this technique is currently being employed by a large number of researchers to estimate the density and thickness of ultrathin layers. The value of the thickness and refractive index it provides is that of the “equivalent” continuous, uniform, isotropic layer in a heterogeneous format. Hence, one limitation of the technique is that this format differs from real-world systems, where self-assembled systems are usually inhomogeneous and anisotropic thin films. Thus where a layer does not have a uniform density profile, is not macroscopically continuous or is anisotropic, the measured values can deviate to varying degrees from those that might be nominally expected.

The obtained refractive index and thickness values are estimated by fitting experimental results (sample length and phase retardations) to a multilayer dielectric continuum electrodynamic model. Hence, different anomalies can be inferred from DPI

results; consequently, we may be vigilant in the critical interpretation of DPI results.<sup>16</sup> Thus, the refractive index is overestimated in the dilute limit and therefore, the layer thickness is underestimated at these experimental conditions. The thickness and refractive index of the submonolayer is properly estimated only when spheres are separated at or below the wavelength (632.8 nm).<sup>7</sup> Furthermore, there are other possible reasons why the layer thickness is underestimated: (A) The waveguide surface is filled from one end –at these experimental conditions, the refractive index is correctly reported for the surface covered, but the thickness is scaled with the amount of the surface covered-, (B) protein is adsorbed at the most favorable sites on the surface, which correspond to dips in the surface, and (C) protein can be deformed at the surface and not have a uniform density profile from the surface.<sup>17</sup> In all cases, the measured thickness is an optical average thickness value and therefore, the extent of the outer layer thickness is underestimated.

Despite all limitations commented here, it is important to emphasize that the DPI measurements have been verified and/or correlated with other techniques. All the relevant references are indeed covered in detail later in the body of the review and in the combined techniques section. So for example thin spun polymer films have been measured with DPI, ellipsometry and atomic force microscopy (AFM) with very close agreement.<sup>18</sup> For polymer multilayer films DPI has for example been compared with ellipsometry by Halthur *et al.*<sup>19</sup> In both these polymer characterization papers the mass deposited was almost identical between the techniques, as was the thickness for thicker layers, whilst the thickness and refractive index determined by DPI was sensitive down to the very first or thinnest layer (unlike the ellipsometry measurement). The dimensions of streptavidin layers have been also compared to the crystal structure by Cross *et al.*,<sup>7</sup> and DPI has been

compared with neutron reflection in several references. These are clear examples of the DPI efficient measurement.

### **2.1.1. Anisotropy**

DPI allows the adlayer anisotropy to be measured in real-time; that is, the attribute of presenting different values of one property depending on the measuring axis. Nevertheless, in some experiments, anisotropy can be considered negligible and consequently estimated values from DPI can be properly calculated presuming that the layer is ideally isotropic. Accordingly, Mann showed that if the particle diameter is much less than the wavelength (632.8 nm), the studied layer can be considered homogeneous.<sup>20</sup> However, anisotropy due to net orientation of bonds/molecular orientation, as with a lipid bilayer, is commonly measured by DPI. The anisotropy can result from the existence of two or more elements with different refractive indices, or the nonrandom orientation of individual molecules. Hence, extreme attention is required when interpreting the results with the aim to accurately estimate the optogeometrical parameters of thin films.

The material nonuniformity can be characterized by birefringence,  $\Delta n$ . This parameter is an optical characteristic of materials whose refractive indices depend on the propagation and polarization direction of light. The most common birefringence is that of materials that have uniaxial anisotropy; that is, layers in which all perpendicular directions to a symmetry axis (optic axis) are equivalent from an optical point of view. In these materials, components of light with different plane polarization (perpendicular and parallel) have unequal refractive indices, denoted  $n_e$  (for extraordinary) and  $n_o$  (for ordinary):

$$\Delta n = n_e - n_o \quad (1)$$

$n_o$  can be estimated from the effective refractive index of the TE mode ( $n_{TE} = n_o$ ). In practice, it is assumed that  $n_{TM} \approx n_e$  because the contribution of  $n_o$  to the effective refractive index of TM mode is small. Thus, the birefringence is the difference between the refractive indices parallel and perpendicular to the surface ( $n_{TM} - n_{TE}$ ). Considering that, the discrepancy between the calculated effective birefringence estimated by DPI ( $n_{TM} - n_{TE}$ ) and the layer birefringence ( $n_e - n_o$ ) is around 2%.<sup>21</sup> Furthermore, either the thickness or the refractive index of the material is considered to be constant in these calculations. Usually, for layers such as lipid bilayers, thicknesses estimated by means of neutron reflection and X-ray scattering are used, or average refractive index values obtained from the bulk material properties.

A typical lipid bilayer has a birefringence of 0.01-0.02 refractive index units. Interestingly, DPI can measure refractive index increments as small as  $10^{-7}$  and can therefore characterize very subtle changes in bilayer structure, revealing mechanisms of interaction that are difficult, or even impossible, to measure by other means. Considering uniaxial films, when  $\Delta n < 0$  (which can arise from molecules aligning flat onto the surface, as opposed to interleaving of materials) the thickness is always underestimated and the mean refractive index is overestimated,  $\geq 10\%$ . Nonetheless, the mass per unit area is underestimated around 1%, given that there is an accidental cancellation of errors.<sup>22</sup> Otherwise, when  $\Delta n > 0$  (which can arise from aligned molecules with higher polarisability in the perpendicular axis, such as lipid molecules in a bilayer), the thickness is overestimated whereas the refractive index is underestimated. Where the birefringence is large this can be a significant effect causing a large overestimation in thickness of more

than 100% or even preventing a uniform layer to be fit to the data. In addition, the estimated mass per unit area has a higher error than that calculated from films with negative values of birefringence. For example for a layer of a highly hydrated protein with a refractive index around 1.36, and a birefringence of 0.06, an error higher than 6% could be reported.

Ideally, sufficient parameters need to be obtained for determining the film anisotropy, but if that cannot be, the approaches adopted by Horvath and Ramsden<sup>22</sup> or those proposed by Coffey *et al.*<sup>17</sup> can be applied for estimating the refractive index and thickness of the adsorbed film. By means of a careful use of these approaches, both these values and the mass per unit area may be estimated correctly.

### **3. Measurement**

In a typical DPI experiment, a silicon chip, which contains three parallel optical channels and provides simultaneous measurement but only allows sample introduction on two, is generally used. The third channel contains a dielectric material with a constant refractive index since it is used as reference channel. This configuration permits the strict control of the assay, ensuring the accuracy of the recorded data. The measurement silicon sensor is positioned on a thermal block, whose temperature interval is between 10 and 60°C, maintaining thermal stability within 1 mK. A fluidic system consisting of an external pump and two high-performance liquid chromatography valves can be coupled with the instrument to allow a controlled continuous flow of the running buffers or samples over the two channels of the chip surface.

In order to measure accurately, it is indispensable to know the starting waveguide structure, which requires the interferometer chip to be calibrated at the beginning of the experiment. This calibration is performed with the aim to obtain the thickness and the refractive index of the device itself, which otherwise would produce errors. In order to perform that calibration two solutions are made to flow over the sensing surface. These reference solutions operate as films with known refractive indices and infinite thicknesses. The transitions between refractive indices of both solutions gives rise to a phase change in both polarizations. The difference between these changes with those expected are taken into account for correction of refractive index and thickness on the sensing waveguide. Consequently, both phase changes are collated against the expected data and thus, any discrepancy is corrected.

Empirically, the interferometer is first calibrated considering the sequential phase changes produced by a solution containing 80% ethanol in water and pure water, whose refractive indices are well known. The reason of using that ethanol solution is because it possesses the maximum refractive index in the water/ethanol phase diagram and so is insensitive to errors in preparation. Similarly, the refractive index of the running buffer is measured from the water to buffer transition. Next, the running buffer is flown until the fringe phase changes of both polarization modes reach a stable baseline (typically after 10 min). As commented above, the refractive index and thickness of the adsorbed film can be estimated by means of the solution of the electromagnetic equations that explain the phase changes of both polarization states.

The potential of DPI measurements has been verified by comparing data with other techniques used in surface science and bionanotechnology. The use of this technique is

gaining popularity as DPI measures instantaneous changes in the refractive index ( $n_i$ , resolution  $\approx 10^{-7}$  units) and dimension ( $Th_i$ , resolution  $< 0.1 \text{ \AA}$ ) of the deposited films, and all simultaneously. Another significant advantage is the use of unlabeled reagents, which clearly simplifies the experimental set up. Additionally, this technique also allows the calculation of other molecular properties from indirect measurements. In this regard, the mass and density of the studied film can be determined using:<sup>23</sup>

$$\rho = \rho_p(n - n_s)/(n_p - n_s) \quad (2)$$

$$\Gamma = \rho * Th \quad (3)$$

where  $\rho$  is the amount of protein within the adsorbed layer in g/mL,  $\rho_p$  the density of protein,  $n_s$  the solution refractive index,  $n_p$  the protein index and  $\Gamma$  is the surface concentration (un-hydrated mass loading per unit area). In order to determine these indirect parameters, it is necessary to specify the adlayer characteristics (such  $\rho_p$  or  $n_p$ ), which can be determined from solution measurements with a refractometer.

Another interesting parameter that can be straightforward calculated from the surface concentration is the area per molecule ( $A$ ):

$$A = Mw/(\Gamma * Na) \quad (4)$$

$Mw$  is the un-hydrated molecular weight of adhered species, and  $Na$  is the Avogadro's number. An alternative analysis, using the thickness to estimate an area per molecule

(assuming monolayer packing of spherical molecules) can be used to calculate the molecular weight of particles on the surface.<sup>105</sup>

**Table 1.-** Comparison of DPI with other analytical techniques.

<b>Technique</b>	<b>Real-time</b>	<b>Close to <i>in vivo</i></b>	<b>Structural detail</b>
QCM-D	Yes	Yes	Medium
SPR	Yes	Yes	Low
X-ray	No	No	Very High
AFM	No	No	High
NR	No	Yes	High
DPI	Yes	Yes	Medium

**Note:** “Close to *in vivo*” means that the sensor can provide information that is similar to those experienced under *in vivo* conditions.

When working in areas such as surface science or materials, it is important to determine the volume fraction of adhered species ( $\theta$ ). This parameter can also be calculated by:

$$\theta = (n^2 - n_s^2)/(n_p^2 - n_s^2) \quad (5)$$

After calculating the parameters above described, not only the gross structure but also the molecular orientation within the adlayers can be inferred. DPI has often been employed to estimate the conformational changes associated with biointeractions, in which case the surface layers are usually biological probes, such as proteins antibodies or oligonucleotides immobilized onto the optical waveguide surface, however they may also consist of polymers, molecular assemblies or nanoparticles etc.

#### 4. Comparison and combination with other techniques

DPI was verified more than a decade ago using standard protein systems. For that, it was compared with NR and X-ray crystallography, obtaining excellent agreement with reported data.<sup>7</sup> In addition, regarding to the values of thickness the precision achieved was around 40 pm.

In Table 1, a comparison of DPI with other analytical techniques is shown.<sup>7</sup> As can be seen, the thickness and density values obtained by DPI have an excellent resolution. Nevertheless, with this technique it is not possible to achieve the remarkable structural detail (atomic coordinates) provided by x-ray crystallography, the. However, DPI allows similar information to be obtained in real-time, as well as in *in vivo* conditions. In the same way, NR provides more structural details within the film, but the measurements cannot be performed in real-time and large equipments are required. Hence, DPI can be used as a complementary tool to other more established analytical techniques, such as NR and X-ray crystallography.<sup>24</sup>

Another group of methods are based on the use of the evanescent field of a beam of laser light to perform the measurements within the adlayer. Among them, SPR is a well-established technique, which has emerged as a key research tool for pharmaceutical development, food quality control, environmental monitoring and clinical analyses.<sup>25</sup> As DPI is one of these techniques, Sonesson *et al.* observed a good agreement between DPI and SPR results and, by extension, with data coming from all evanescent field techniques.<sup>26</sup> The main advantage of DPI is that it measures simultaneously the refractive index and thickness of the studied layer in real-time, whereas SPR is more exact in studies on initial adsorption kinetics. This is so because SPR performs the measurement on a very small area (0.26 mm<sup>2</sup>), whereas DPI measures average values along the entire length of chip (15 mm); consequently it takes longer for the concentration on the sensing surface

to be homogeneous. Furthermore, the cell volume in the DPI is around 2  $\mu\text{L}$ . Hence, if the flow rate is around 10  $\mu\text{L}/\text{min}$ , the cell volume is replaced with the measurement solution in 12 s. Accordingly, initial measurements in DPI not only refer to adsorption kinetics but also to the replacement of the bulk solution.<sup>27</sup>

In SPR, the quantification of the phase angle allows only the thickness or refractive index of the adhered molecules to be quantified. Dual measurement optical approaches (such as SPR, ellipsometry or circular dichroism) measure both parameters in separate assays, which forces the researcher to infallibly replicate infallibly the same process in two different assays. On the contrary, DPI allows the thickness and refractive index to be measured almost simultaneously, offering a substantial advantage over other optical methods.

Unlike other surface characterization techniques such as QCM-D and SPR whose measurements offer only separately estimations of the mass, density, or thickness of a thin film, DPI is an optical technique that actually provides an exact method to measure simultaneously these parameters at solid-liquid interface, as commented above. Whereas the microbalance is a well-established technique, which detects both hydrated mass and structural parameters of the adlayer in real-time, DPI has emerged as an original unlabeled analysis technique that employs a simplified slab waveguide interferometer to measure the dry mass of a thin film. Here, it is important to emphasize that, in both techniques, the step to a precise mass determination requires the introduction of several assumptions and a model. Both masses are not directly measured but correlated to observables that are measured.

Using QCM-D, the adlayer's mass, taking into account the solvent, is estimated. The solvent mass is due to the viscous drag, the hydration or the existence of solvent cavities in the adlayer. On the contrary, DPI resolves only the mass of the unhydrated

adlayer, excluding the mass of any incorporated solvent. This mass is proportional to the amount and molecular weight of the adsorbed biomacromolecules. Accordingly, by comparing these two measurements, two major conclusions can be drawn: (A) the amount of hydrodynamically coupled water<sup>28</sup> and (B) the effective film density can be estimated with high accuracy. The resulting thickness of adsorbed film can be also measured through the layer density, which agrees with values measured by other analytical methods.

In addition to mass, QCM-D also measures the energy dissipation of the oscillator, which allows soft films to be analyzed. The frequency measurement of these peculiar films is not proportional to the mass changes and accordingly, the mass calculus may be carried out considering the dissipation factor. This factor is a quantitative parameter of the conformation, and supramolecular structure, of the adlayer. Thus, Mashaghi *et al.* demonstrated that the changes of this dissipation factor are correlated with the birefringence changes detected by DPI.<sup>21</sup> It is possible to say that QCM-D is a complementary method to DPI for measuring the supramolecular conformation of adsorbed films.

Attenuated total reflectance-FTIR spectroscopy (ATR-FTIR) has been extensively used for studies of biological membranes.<sup>29</sup> Hence, combining ATR-FTIR with DPI for the characterization of these adlayers will be a logical next step.<sup>30</sup> In this combination, DPI provides information on the tertiary structure of proteins, whereas the infrared spectroscopy is employed to learn about its secondary structure (e.g.  $\beta$ -turning,  $\alpha$ -helix or sheets). All this information is essential for a better understanding of biomolecular interactions.

Macroscopically large areas are chosen in DPI in order to minimize the effect of inhomogeneities and changes in the adlayer. Thus, microscopy methods, such as AFM,

are typically employed together with DPI for characterizing these inhomogeneities.<sup>31</sup> AFM is a versatile surface characterization technique with an extremely high spatial resolution, which enables the study of biological and even living organisms providing three-dimensional topographical images. Hence, when both techniques are combined, AFM is used to estimate the three-dimensional structure of molecules and examine their surface shape, whereas the interferometer measures average monolayer thicknesses. These studies provide a new way to study the protein conformational dynamics, which is critical in how biological molecules exert their function and regulate biological processes.

DPI has been also used to detect crystallization processes, given that the loss processes that occur on its sensing surface have a significant impact on the measured signal. Accordingly, the DPI-dialysis tandem allows crystallization processes and amorphous depositions to be discriminated.<sup>32</sup> This tandem is a very effective tool for optimizing crystallization conditions, for studying crystallogenesis or for differencing between microcrystallization and amorphous precipitation in real-time.

## **5. Bioreceptor immobilization**

### **5.1. General remarks**

The development of new methodologies for immobilizing biomolecules at the surfaces of sensing chips has undergone significant advances in recent years and has become an integral part of research in the field of biotechnology.<sup>33</sup> In this regard, the bioreceptor anchoring has become one of the key aspects for developing an effective biosensor. The sensor chip used in DPI experiments is composed of four stacked dielectric waveguides of silicon oxynitride (SiON) onto a silicon surface. The reference and sensing waveguides

are separated by means of an insulator, the sensing waveguide being the unique element in contact with the solution.

Many other materials have also been studied for fabrication and characterization of waveguides.<sup>34</sup> SiON is an important aspirant to fabricate on-chip delay lines, because of its compatibility with very-large-scale integration processes. Furthermore, the waveguides fabricated with SiON have a lower index contrast, and therefore losses, than waveguides composed of silicon, allowing longer optical delays. In contrast with the stratified metallic optical waveguides, the oxynitride has a high refractive index. This allows the index contrast to be tailored depending on the desired application.

Accordingly, many efforts have focused on the chemical functionalization of the SiON upper layer. The immobilization processes have been planned in order to maximize the surface density of probes on the chip and at the same time, minimizing the nonspecific binding to the support. Also, it is important that the attachment does not affect the biological activity of the biorecognition element.

**Table 2.-** Summary of immobilization strategies. Specific characteristic of the protein (Pr) or DNA immobilization strategies are highlighted.

<b>Immobilization Strategies</b>			
<b>Immobilization strategy</b>	<b>Description</b>	<b>Advantages</b>	<b>Disadvantages</b>
Physical adsorption	Immobilization based on weak interactions (hydrogen bonds, intercalation, van der Waals and $\pi$ - $\pi$ interactions, hydrophobic interaction).	Single step immobilization No coupling reagents required Universally applicable (only Pr) No modification required (only Pr)	Random orientation No control over distribution Reversible immobilization Protein leaching from support (only Pr)
Biochemical affinity	Immobilization via non-covalent interactions, e.g. biotin-avidin (or streptavidin).	Oriented immobilization	Possible loss of bioactivity Coupling reagents required

Covalent	Chemical bond formation between protein and support groups	Possible oriented immobilization Homogeneously oriented layers Spatial surface patterning Stable immobilization (only DNA)	Modification required Coupling reagents required
----------	--	---	---

---

## 5.2. Protein attachment

Protein immobilization onto solid supports is fundamental for the fabrication of microarrays, biosensors, continuous flow reactors systems and nanotechnology. Recently, much attention has been paid to the search of oriented protein immobilization methodologies, which allow the immobilized proteins to be oriented, preserving the binding site accessible.

In general, three different approaches have been used to link proteins to solid supports (Table 2). The first one involves methods which rely on physicochemical adsorption phenomena,<sup>35</sup> the second one is based on the use of bioaffinity interactions, whereas the third strategy implicates the formation of stable covalent bonds.<sup>36</sup>

### 5.2.1. Physical adsorption

Classically, non-covalent immobilization of proteins on solid surfaces is achieved by physical adsorption, making use of van der Waals forces, hydrophobic and electrostatic interactions and ionic bonds. The main benefit of this strategy is that additional steps are not required, and it is applicable to any protein. However, physical interactions are generally weak and sensitive to changes in experimental conditions, giving low control over the orientation of the proteins. As a result, conformational changes or denaturation can occur, which involves media contamination and loss of activity. Physical adsorption

is also affected by the charge on the protein and the surface, so may vary with the pH of the buffer and the isoelectric point of the protein. Furthermore, since this approach does not allow the packing density to be controlled, protein activity can be negatively affected by steric congestion.

Hence, this strategy may result in some cases inappropriate in terms of robustness and recyclability.<sup>37</sup> Despite these disadvantages, this methodology has been widely used to immobilize proteins onto silicon<sup>38</sup> and other surfaces.<sup>39</sup> Another efficient approach commonly used in the generation of protein nanoarrays is based on the immobilization through self-assembled monolayers (SAM), which generally are covalently attached to the solid surface. In this strategy proteins are immobilized by means of polar, hydrophobic or electrostatic interactions, using positive or negative SAMs (charged amine and carboxyl groups, respectively).<sup>40</sup>

### **5.2.2. Biochemical affinity**

Another popular coupling route is based on the strong interaction between biotin and avidin (or streptavidin),  $K_a \approx 10^{15}$  M. This rapid interaction is independent on organic solvents, pH and temperature. Biotin, which is a water-soluble B-vitamin, is composed of a tetrahydroimidizalone fused with a tetrahydrothiophene ring with a valeric acid substituent. Avidin, streptavidin and neutravidin are tetrameric glycoproteins, which can bind up to four molecules of biotin. Due to its simplicity and versatility, the biotin-streptavidin methodology has been commonly used in different biotechnological applications.<sup>41</sup> This strategy requires a prior step of protein conjugation with biotin, followed by the linkage with avidin (or streptavidin) which is attached to the surface, or

vice versa. Both biotin and (strept)avidin can be conjugated to other proteins without loss of affinity and the need of a biotin labeling step. Biotinylation can also be site directed, enabling oriented immobilization of the protein.

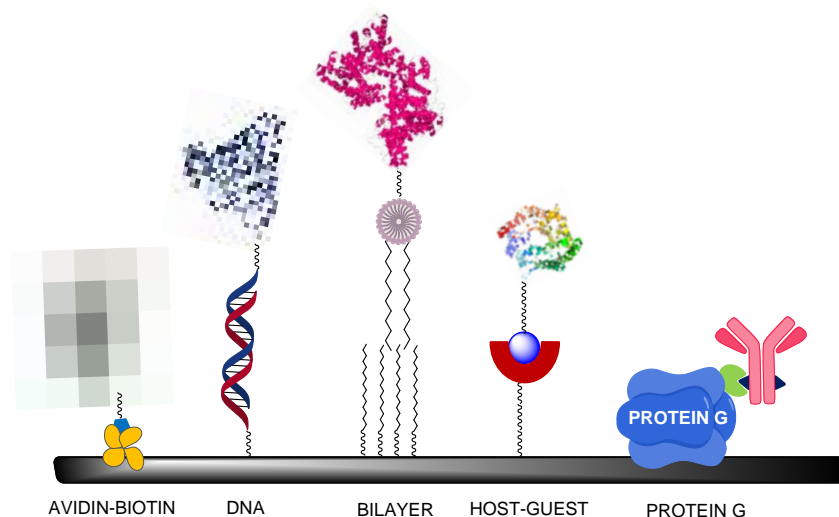


**Figure 6.** Different protein immobilization approaches based on biochemical affinity.

The above-commented immobilization processes can also take place by other different bioaffinity interactions (Figure 6). In this regard, taking advantage of the strong interactions between complementary single-stranded acids, deoxyribonucleic acid (DNA)-directed immobilization has also been used. This strategy requires a prior step of binding of the protein to a single-stranded DNA (ssDNA), followed by hybridization with a complementary ssDNA of sequence which is attached to the surface.<sup>42</sup> Different approaches using hybrid bilayer membranes,<sup>43</sup> and host-guest complexes<sup>44</sup> have been also described to immobilize proteins. Finally, another approximation is based on the high affinity and binding specificity of Proteins A and G, which allows the capture of antibodies in an oriented manner.<sup>45</sup>

### 5.2.3. Covalent immobilization

Covalent immobilization provides the best approach to combine longevity of the biofunctionalized surface with a high sensitivity due to the specific orientation of the protein. Many functional groups are available in proteins for immobilization processes, such as the side chains of amino acids. In this regard, a variety of organic reactions have been extensively used.<sup>46</sup> The most common method involves firstly the use of a reactive intermediate to functionalize the SAM.<sup>47</sup> A typical approach is based on the use of organosilanes to covalently attach proteins onto silicon materials.<sup>48</sup>

Most methodologies are based on chemical reactions between the amino acid residues and a functional group anchored on the surface. Accordingly, chips containing active ester moieties easily react with lysine residues by means of the amine groups, using N-hydroxysuccinimide (NHS) as an activating reagent for esters. However, modest immobilization yields are achieved due to the low stability of NHS esters in aqueous conditions. Aldehyde groups can be also used instead of ester moieties. They also react with the amine groups of the proteins to generate imines,<sup>49</sup> which are subsequently transformed into a stable secondary amine bond by means of its chemical reduction. Furthermore, these amines can also react with epoxide-functionalized materials, which are stable to hydrolysis under neutral conditions.<sup>50</sup> The thiol group of cysteine is usually employed to immobilize biomolecules through the thioether bonds with  $\alpha,\beta$ -unsaturated carbonyls. Also, the nucleophilicity of the thiol group can be used to bind NHS esters and epoxides. The acidic glutamate and aspartate amino acids can be converted *in situ* to active esters by means of carbodiimide coupling agents (such as 1-ethyl-3-(3-dimethylaminopropyl)carbodiimide) and NHS.<sup>51</sup>

Recently, bioorthogonal chemical reactions, which allow small-molecule probes to be attached regioselectively to proteins, have emerged as a relevant and attractive tool for site-specific labeling, and for immobilization, of proteins.<sup>52</sup> Typically these methods are based on specific reactions, e.g. thiol-maleimide reaction,<sup>53</sup> thiol-ene “click reaction”<sup>54</sup> and variants,<sup>55</sup> Staudinger ligation reaction<sup>56</sup> and Diels-Alder reaction.<sup>57</sup> A good very recent example of covalent immobilization, which assesses a variety of methods and orientations for antibody immobilization, has been reported by Song *et al.*<sup>58</sup>

### **5.3. DNA attachment**

DNA is an essential biological material whose base sequence controls the heredity of life. It is therefore of potential interest, *inter alia*, to design oligonucleotide probes for the detection of tumor gene. DNA represents a fundamental object of research in biochemistry, biology and life science and it has been recently used with potential applications in many research areas, such as gene therapy,<sup>59</sup> bio-nanotechnology,<sup>60</sup> bio-sensing,<sup>61</sup> bio-engineering,<sup>62</sup> drug delivery<sup>63</sup> and molecular biology.<sup>64</sup> In the last decades, biomedical studies have focused their efforts on the development of selective and sensitive techniques for DNA detection. The immobilization of DNA can take place mainly by means of three groups of methods, namely physisorption, covalent immobilization, and immobilization through avidin-biotin interactions (Table 2).

#### **5.3.1. Physical adsorption**

DNA physisorption is the simplest attachment technique, given that no DNA alteration is required. It is immobilized by simply submerging surfaces in DNA-containing solutions.

Thus, DNA is attached by weak interactions, e.g. van der Waals interactions, groove bindings, intercalations,  $\pi$ - $\pi$  interactions, hydrogen bonds or hydrophobic interactions. Although DNA adsorbs very poorly to the surface, with negative charge, of cleaned DPI chips, it has been efficiently immobilized through these interactions onto several substrates,<sup>65,66</sup> with surface coverage for the DNA layer around 95 %. As this approximation do not permit to control DNA coverage, the steric congestion results a disadvantage as high immobilization densities do not necessarily imply high hybridization efficiencies.

### **5.3.2. Avidin-biotin interaction**

The approach of DNA immobilization by means of bioaffinity reactions is commonly employed. Due to the specificity and strength of this bond, the avidin-biotin interaction is one of the most extensively affinity pairs used in cellular, molecular and immunological assays. Using this specific binding strategy, which is based on strong non-covalent interactions, DNA is usually attached, directly or via a flexible spacer, to the comparatively small biotin moiety which then forms a strong bond with surface-bound avidin or streptavidin.

Despite the use of this strong interaction for the attachment of DNA requires the use of biotin-modified oligonucleotides and do not permit the chip reusability, the avidin-biotin mediated coupling is the simplest methodology for attaching oligonucleotides. This strategy has been successfully applied to different solid supports.<sup>41,67,68,69</sup>

### **5.3.3. Covalent immobilization**

The covalent attachment is the preferred approach because of its high reproducibility, probe directionality, reduced background noise, high hybridization efficiency and controlled immobilization. However, for this immobilization strategy, oligonucleotides must be chemically modified with a functional group in order to induce the covalent attachment on the solid surface. In this regard, self-assembly with organofunctional alkoxy silane molecules is the most common strategy for functionalizing glass and silicon chips.<sup>70</sup>

Among the wide variety of organosilane reagents, the most frequently used are 3-aminopropyltriethoxysilane (APTES) and isocyanatepropyltriethoxysilane (ICPTS). These isocyanates bind with amine-modified oligonucleotides, forming the isourea groups. In the last decade, the use of 3-mercaptopropyltriethoxysilane (MPTS) and 3-glycidoxypropyltrimethoxysilane (GOPTS) has been also implemented in the functionalization of sensing devices. The use of MPTS allows thiolated oligonucleotides to be immobilized onto the surface by means of disulfide bonds or by the “thiol-ene” click (TEC)<sup>71</sup> or “thiol-yne” (TYC) reaction<sup>72</sup>. Another approach for DNA immobilization is the epoxy chemistry, which is stable in aqueous solutions and allows several nucleophiles to be bound, e.g. sulfhydryl groups or amines. It is noteworthy that its immobilization based on “thiol-ene” reaction and epoxy chemistry have allowed a site-selective attachment through the use of a photomask and UV light (Figure 7).

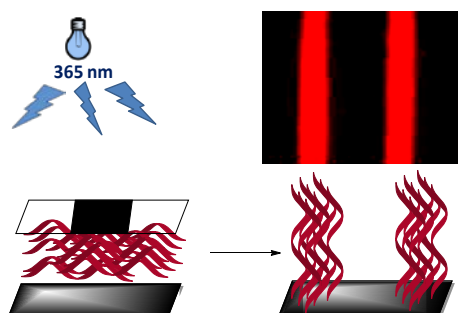


**Figure 7.** Site-selective immobilization through a photomask.

## **6. Applications**

The validity of a technology is directly related to its applicability. In this regard, this is referred to the ability to efficiently solve problems difficult to be managed by other technologies. Accordingly, DPI is an effective, label-free methodology with extensive use in biophysics and surface science. One potential challenge solved by means of this technology is the development of a sensitive analytical technique able to monitor in real-time the connection between molecular function and structural changes. Furthermore and due to its sensitivity, DPI is emerging as a promising analytical tool to implement legislation in different fields, e.g. forensics, drug discovery, environmental and food sciences.

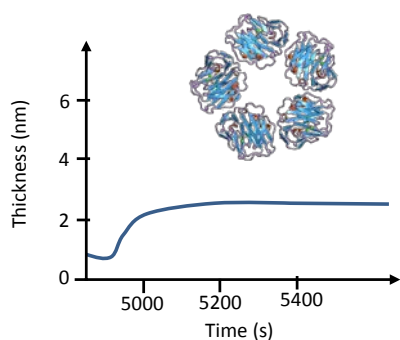
### **6.1. Protein Studies**

Proteins are extremely complicated structures whose proper behavior is vital to biological systems and therefore, their malfunction is closely related to most diseases. Looking at important roles proteins play in living systems, it is natural for human interest to delve into exploring structure, function, working mechanisms and other aspects related to these biological entities. The study of solution-phase interactions with attached proteins is of utmost importance, mainly for the pharmaceutical industry.<sup>73</sup> In this regard, DPI has been widely used through the last decade as a powerful technique to examine the protein sensing with quantitative metrology.

### 6.1.1. Characterization and conformational changes

Protein characterization is a pre-requisite for the discovery and development of new pharmaceuticals and biomarkers. For that, researchers are continuously demanding more effective analytical approaches to study proteins in a more native environment. DPI allows the determination of the protein density and its structural parameters in real-time, and, as a consequence, researchers are increasingly employing this technique in the protein characterization, a vital branch of knowledge in proteomics.<sup>74</sup>

In an early publication about this topic, DPI data combined with AFM imaging was employed to plot the surface nanostructure and to estimate the size of C-reactive protein,<sup>75</sup> a protein used as a marker of inflammation associated with cardiovascular diseases. AFM showed a pentagonal torus (doughnut-shaped) structure, whose dimensions were estimated by DPI and AFM analysis (Figure 8). Thus, the estimations of the protomer diameter (36 Å), pore diameter (3.5 nm) and outer diameter (11 nm) suggested how C-reactive protein molecules were recognized on the sensor chip. This pentagonal structure was further dissociated into monomers or aggregates in acid or basic medium. However, protein subunits were only rearranged at very acidic solutions. Taking into account the subclinical chronic inflammation and proinflammatory effect, these pH-induced structure changes could be related to the arteriosclerotic vascular disease.<sup>76</sup>



Measurement	DPI	AFM
$\Gamma$ (ng/nm <sup>2</sup> )	1.48	----
A (nm <sup>2</sup> )	128	125
Th (nm)	3.18	3.03

**Figure 8.** Surface characterization parameters of an immobilized C-reactive protein monolayer.

A similar publication showed the applicability of DPI to monitor the conformational changes which were undergone by prion protein after the addition of  $\text{Cu}^{2+}$ .<sup>77</sup> Insignificant alterations in the structure of protein were determined, indicating that interferometry has a great interest for studying prion diseases, as these differences provided confirmation that the copper-prion complex and the copper charged apoprion are different, structurally speaking. In agreement with this, DPI showed alterations between copper charged prion proteins, depending only on the copper binding process. The authors concluded that the structure of the copper-prion complex was that of the normal cellular isoform and not prion in the Scrapie form.

In 2007, Karim *et al.* reported an interesting application for the measurement of conformational changes on covalently immobilized transglutaminase when binding  $\text{Ca}^{2+}$ .<sup>78</sup> The authors were able to quantify the structural changes in connection with the calcium concentration in solution -these films contract around 0.5 nm depending on the calcium concentration- and to calculate the affinity constant (0.9 mM).

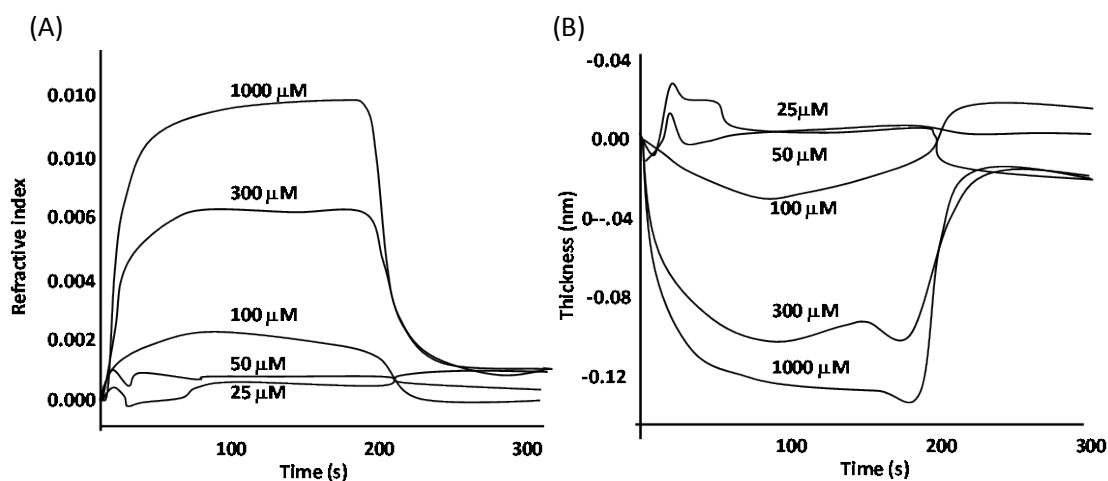


**Figure 9.** Shifts in the refractive index (A) and thickness (B) of the film of recombinant matrilin-3 A-domain as a function of Zn<sup>2+</sup> concentration.

Similarly, conformational changes of the A-domain of the matrilin-3 (a protein involved in bone growth) in the presence of Zn<sup>2+</sup> and Ca<sup>2+</sup> were monitored in real-time, as part of a deep and complex characterization study of this protein domain and their consequences in the basis of genetic bone disorders in humans.<sup>79</sup> The binding of Zn<sup>2+</sup> to the immobilized protein increased its density, so decreasing its thickness (by 0.12 nm), allowing the estimation of a dissociation constant (0.75 mM) for the binding of this cation (Figure 9), whereas the addition of Ca<sup>2+</sup> did not produce a significant effect.

An analogous study was reported by Coan *et al.* for measuring the Calmodulin M interaction with Ca<sup>2+</sup> and the small molecule trifluoperazine (a typical antipsychotic of the phenothiazine chemical class).<sup>4</sup> It was observed that Ca<sup>2+</sup> increased the protein thickness around 0.05 nm and decreased density by 0.03 g/mL, whereas trifluoperazine increased both density (0.01 g/mL) and thickness (0.05 nm). Thus, these authors showed, for the first time, that DPI allows ligands with distinct structural forms of action to be

identified and classified. It is worth mentioning that these variations are extremely small, but DPI allows them to be distinguished.

In 2009, Gupta *et al.* established a ratio between the lengths of aliphatic chains bound to acyl carrier protein, which is vital in the biosynthesis of both polyketide and fatty acid, and its size.<sup>80</sup> Interestingly, it was observed that every two carbon atoms of the attached aliphatic chain produced an enhancement in the volume around  $60 \text{ \AA}^3$ . These studies allow conformational shifts in mutant acyl carrier proteins to be investigated in relation with their physiologic behavior.

Zwang *et al.* explored the degree of desolvation happening when small molecules bound to immobilized bovine serum albumin (BSA).<sup>81</sup> The authors observed that desipramine (a tricyclic antidepressant) interacted tightly with BSA ( $0.195 \text{ nM/cm}^2$ ) and displaced bound water molecules. However, caffeine bound to BSA ( $0.134 \text{ nM/cm}^2$ ) without displacing water, while salicylic acid bound in a much lower amount ( $0.065 \text{ nM/cm}^2$ ), but induced BSA desolvation because of the binding-induced conformational changes (Figure 10).

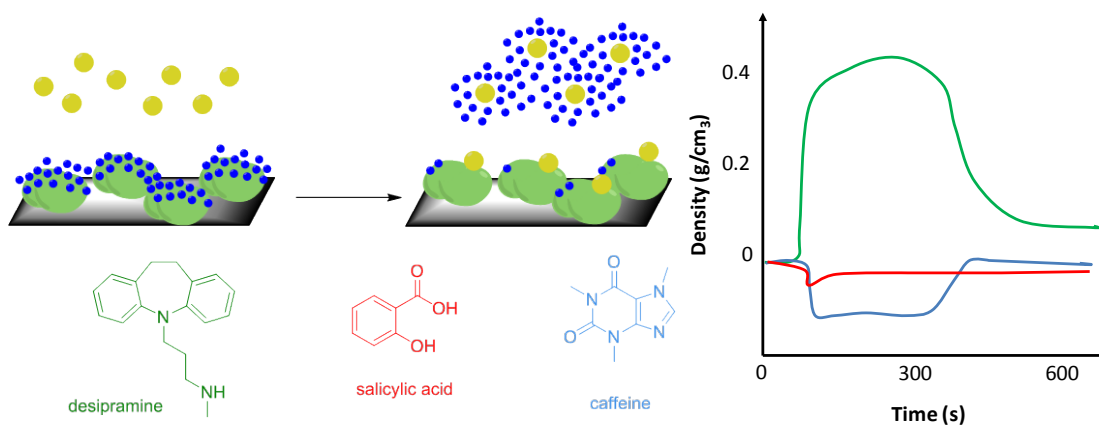


**Figure 10.** Effect of caffeine (blue), salicylic acid (red) and desipramine (green) on the density of adsorbed BSA.

### 6.1.2. Crystallization monitoring

Crystals of macromolecules have become keystones of molecular biology and the crystallization of proteins has become an excellent tool to obtain information about the three-dimensional protein structure.<sup>82,83</sup> A very interesting application of DPI is the identification of protein crystal nuclei on the chip surface and monitoring the crystal growth. This measurement is possible on the basis on the phase changes and the fringe contrast, which decrease when microcrystals are formed on the chip surface, enabling to find the best conditions leading to the formation of protein crystals.

Usually, the phase shifts happen during the DPI measurement, but the contrast does not change considerably. Nevertheless, the loss of light from the waveguide can modify that contrast. As commented above, this is due to the optical absorption or the existence of surface structures, which couple or scatter light out of the waveguide. The existence of these structures is the result of crystallizing proteins.<sup>84</sup> Boudjemline *et al.* shows how DPI allows early protein crystallization processes to be detected in real-time, given that the two detection parameters (contrast and phase) change due to this accumulation process.

In 2011, Boudjemline *et al.* used the optical properties of the DPI device to establish the optimal conditions for the crystallization of several proteins (lysozyme, catalase, thaumatin, rat dynamin and xylanase).<sup>32</sup> The precipitation conditions were modulated by means of a dialysis method directly coupled on the measurement chip,

allowing shifts in the protein solution to be detected at the same time with the adjustment of the precipitant concentration. Particularly, DPI was employed to plot the initial protein adsorption to the sensing surface, precipitation, crystallization, nucleation, aggregation onto the surface and salting-in, against the precipitant amount. At this point, it is important to emphasize that nucleation-crystallization and amorphous aggregation events could be clearly distinguished.

In a recent work, another application of the DPI-dialysis tandem was reported in combination with other techniques for crystal generation, growing and characterization.<sup>85</sup> In this extensive study, crystal growth was monitored by dynamic light scattering, whereas UV fluorescence was employed to distinguish protein from salt crystals and counter diffusion for screening precipitants. The latter was used in combination with DPI in order to discriminate between nucleation and other solid-state transitions (Figure 11). The DPI-dialysis tandem has a wide range of applications including the crystallization phase space mapping or the screening of additives. Accordingly, the authors could monitor the nucleation and was successfully used to detect the crystallization of thaumatin from *Thaumatococcus daniellii*, bovine liver catalase, and hen egg-white lysozyme.

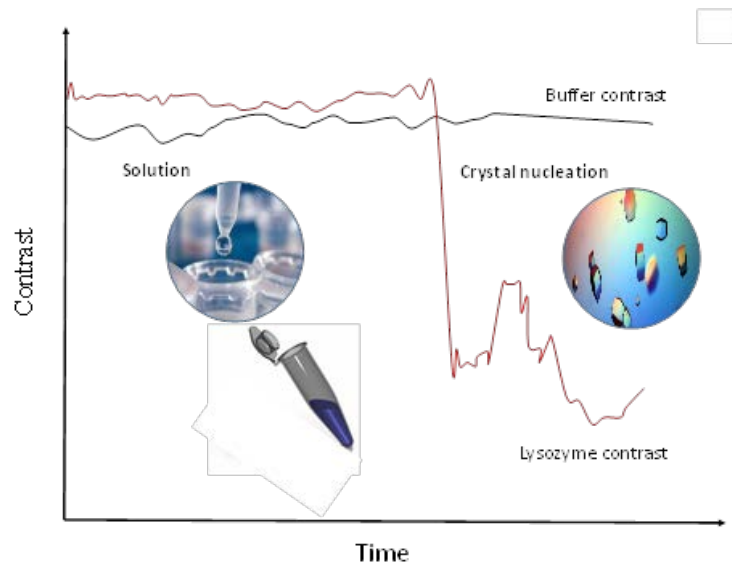


**Figure 11.** Monitoring the nucleation of lysozyme crystals.

### 6.1.3. Adsorption

Since its origins, DPI has emerged as a suitable technique to perform protein adsorption studies, as it has led to a better understanding of the complex protein adsorption processes. Indeed, in 2004, an early report about the bovine serum albumin (BSA) adsorption was described and the pH-dependent structural changes were measured.<sup>86</sup> Hence, the adsorbed BSA surface structure at the different tested pHs (3, 5 and 7) could be deduced from data obtained for mass and thickness increments. Interestingly, the BSA adsorption mechanism could be deduced by combining the aforementioned parameters with the known structure of the bulk solution and the adsorption rates previously calculated. Moreover, it was observed that when the pH was cycled, conformational changes were reversed, indicating that denaturation of protein did not take place on the SiON chip.

The same authors reported a similar work using lysozyme, which is a protein that damages bacterial cell walls.<sup>87</sup> The effect of protein concentration on the adsorption

process was tested at pH 4 and 7. At pH 4, it was observed that layers formed ranged from 1.4 to 4.3 nm thickness, and from 0.21 to 2.36 ng/mm<sup>2</sup> mass covering, whereas the layer thickness changed from 1.6 to 5.4 nm at pH 7, but surface coverage was much higher (from 0.74 to 3.29 ng/mm<sup>2</sup>). These observations indicated a deformed monolayer at low lysozyme concentrations and a double layer for high ones. Furthermore, pH shifting from 4 to 7 resulted in a slight partial reversion of the adsorption behavior. The results achieved were consistent with previously published ones, and showed that DPI can complement NR data.

In 2007, the results of Sonesson *et al.* supported the employment of both DPI and SPR as complementary tools to study the protein adsorption.<sup>27</sup> In this work, lipases from *Thermomyces lanuginosus* were adsorbed on C18 surfaces. The surface densities measured by both analytical tools agreed with adsorption isotherms, the saturation density being around 1.30-1.35 mg/m<sup>2</sup>.

The same research team employed DPI and confocal microscopy for measuring the activity and adsorption of *Thermomyces lanuginosus* lipase on surfaces of different hydrophobicity.<sup>88</sup> As a result, it became clear that this lipase has higher attraction for hydrophobic surfaces (1.90 mg/m<sup>2</sup>) than for hydrophilic ones (1.40–1.50 mg/m<sup>2</sup>). Nevertheless, the linear trend of the refractive index with the surface density showed that the lipase structure did not depend on the surface coverage. Furthermore, a higher activity was found on hydrophilic surfaces, suggesting a site-directed lipase immobilization.

The effect of contamination in the protein bovine submaxillary gland mucin was investigated by Lundin *et al.*<sup>89</sup> Purified mucin exhibited very low affinity for silica and

mica under the studied conditions. First, mucins were adsorbed on the mica surface in an extended conformation with tails spreading out the solution. Those tails were later compacted into a layer of around 10 Å after a high load. Bovine submaxillary gland mucin gave rise to thicker compressed layers (35 Å), although a similar extended layer structure was observed. After adsorption of mixtures of purified mucin and BSA on mica, a 9 wt% albumin content provided a similar layer thickness as mucin. Data from X-ray photoelectron spectroscopy (XPS) indicated that the percentage of surface covered by purified mucin was scarce (5 wt %). Finally, adsorption from an equimolecular mixture of mucin and BSA showed the dramatic effect of mucin on the adsorbed thickness and structure, even for small amounts of mucin present in the mixed layer. Thus, this investigation revealed the strong influence of the purity of mucin on the surface density and layer structure.

In 2011, Cowsill *et al.* studied globular proteins adsorption and compared data for BSA with NR applying the same conditions in both techniques.<sup>90</sup> The Langmuir adsorption model was the one used to quantify the BSA adsorption process under diluted conditions (below 0.5mg/mL), whereas the kinetics of random sequential adsorption was employed above 0.5 mg/mL. Layer thicknesses obtained with both analytical tools were very similar, as shown in Figure 12. It was observed that, globular proteins overlap at high surface densities, while the structure of these proteins collapses at low surface densities and consequently, they wet the substrate.

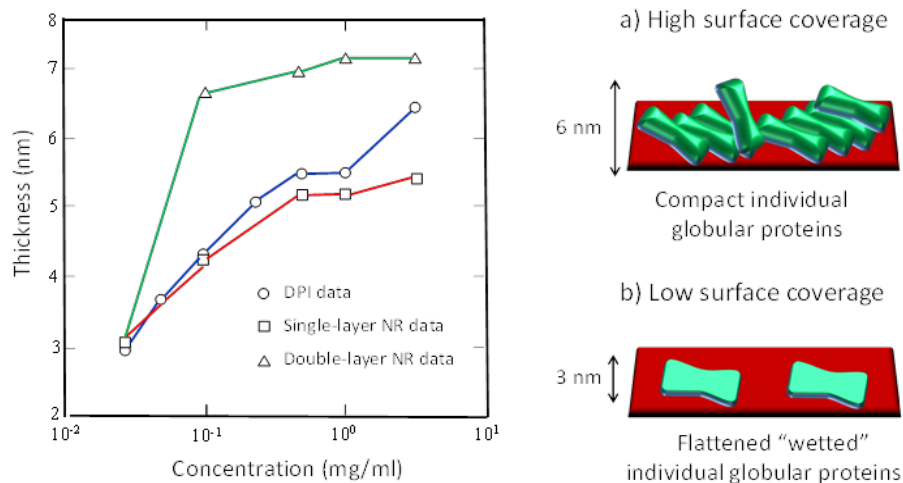


**Figure 12.** Impact of the equilibrium surface coverage on the structural conformation of globular proteins.

An original DPI study was carried out by Zhai *et al.* for monitoring conformational changes associated with the  $\alpha$ -Lactalbumin adsorption on the oil/water interface, in combination with front-face fluorescence spectroscopy and synchrotron radiation circular dichroism spectroscopy (CD).<sup>91,92</sup> In this study, the protein was adsorbed from a bulk buffer to a C18-modified chip, and great differences were found in adsorption results. For hydrophilic adsorption, thickness, mass and density were around 2 nm, 0.3 mg/m<sup>2</sup> and 0.18 g/mL respectively, values consistent with the crystal structure of the lactalbumin. However, protein adsorbed on the C18 hydrocarbon surface resulted in 1.1 nm thickness, 1.2 mg/m<sup>2</sup> mass and 1.1 g/mL density, indicating a strong conformational change (Figure 13). Accordingly, the authors concluded that the studied proteins adopted a helix-rich secondary structure at the oil/water interface.

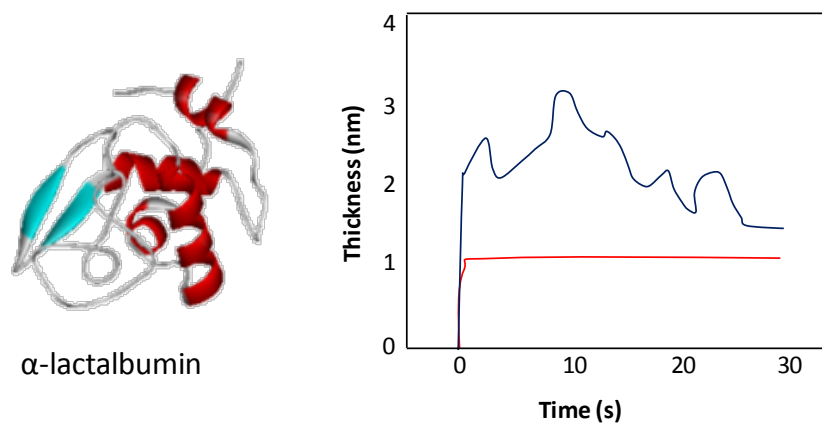


**Figure 13.** Real-time changes thickness of  $\alpha$ -La (100  $\mu$ M, pH 3) attached to a SiON surface (blue) and  $\alpha$ -La (10  $\mu$ M, pH 7) attached to a C18 surface (red).

DPI is a very valuable tool to investigate adsorption phenomena for proteins with peculiar adsorption properties, such as mussel adhesive proteins. The adsorption of *Mytilus Edulis* Foot Protein (Mefp-1), which is the most important one, was studied by Krivosheeva *et al.* in 2012.<sup>93</sup> The protein was directly adsorbed on an unmodified DPI chip, and the kinetics and final amount of adsorbent protein were studied at different pH values. At pH 3, with the surface nearly uncharged, the amount of adsorbed protein was very low, whereas, at higher pH, the adsorbed amount increased, and the protein behaved as a polyelectrolyte. Hence, the authors concluded that the adsorption kinetics and rate were mainly conducted by electrostatic interactions.

Mussel adhesive proteins is a natural glue produced by marine mussel, which allows surfaces to be bound in water. The employment of these proteins (e.g. the Mefp-1) for modifying surfaces requires generating dense and resistant films under changing conditions. Accordingly, DPI was used to study the adoption of Mefp-1 aggregates and non-aggregated samples. It was concluded that the adsorption of a non-aggregated sample involved lower surface density, smaller thickness and similar hydrophobicity compared

to the same layer generated by a sample with small aggregates.<sup>94</sup> Furthermore, this adsorbed Mefp-1 film was more resistant to desorption than the same layer generated through a synthetic cationic polyelectrolyte with similar charge density. Hence, these data indicated that the Mefp-1 has higher non-electrostatic affinity to the surface than the cationic polyelectrolyte.

The same research team have described another recent application for evaluating the kinetics and the equilibrium state of adsorption processes (and desorption), employing proteins with interesting surface properties.<sup>95</sup> Two class of hydrophobins with similar structure (HBI and HBII, approx. 100 aminoacid residues, Mw 7.2 and 7.5 kDa respectively) were efficiently adsorbed and desorbed on the unmodified DPI chip at different flow rates, and the continuous measurement of thickness, mass and refractive index provided remarkable results. The behavior was different for the two species: the amount of HBII adsorbed was always higher than that of HBI; the adsorption process of HBII is weakly cooperative at low surface densities, tendency not shown by HBI. On the other hand, desorption of both proteins from the surface was observed at stopped flow in presence of free protein in the solution, being higher for HBII. This suggests that hydrophobins in solution interact with the adsorbed ones, e.g. forming aggregates, and remove them from the surface.

In a recent study, the information obtained from DPI was contrasted with data from quartz crystal microbalance with dissipation monitoring (QCM-D) to better understand the lysozyme adsorption.<sup>16</sup> As QCM-D measures the adsorbed hydrated film, the adhered solvent mass can be estimated through the subtraction of the mass measured by DPI (un-hydrated mass) from the mass measured by QCM-D. The authors surprisingly

found that the coupled solvent was very important as it was closely related to the behavior of proteins at surface,<sup>96</sup> and they concluded that the orientation of the adsorbed lysozyme depend on the surface density (Figure 14). Lysozyme was observed to be adsorbed from sparse monolayer to multilayer coverage. Interestingly, these monolayers had a surface density around 2-3 ng/mm<sup>2</sup>, with thicknesses between 3 and 4.5 nm, which depend on the molecular orientation at the interface. At these experimental conditions, the film hydration is about 50 wt%. Thus, and as the protein surface density decreased by 5-fold, this datum indicates that the lysozyme molecules are deformed during their irreversible adsorption. Otherwise, multilayers were generated when the surface density was higher than 3 ng/mm<sup>2</sup>. This DPI-QCM-D tandem was so validated to obtainer information about the film wt% solvation, allowing the steps of the lysozyme adsorption to be modeled.

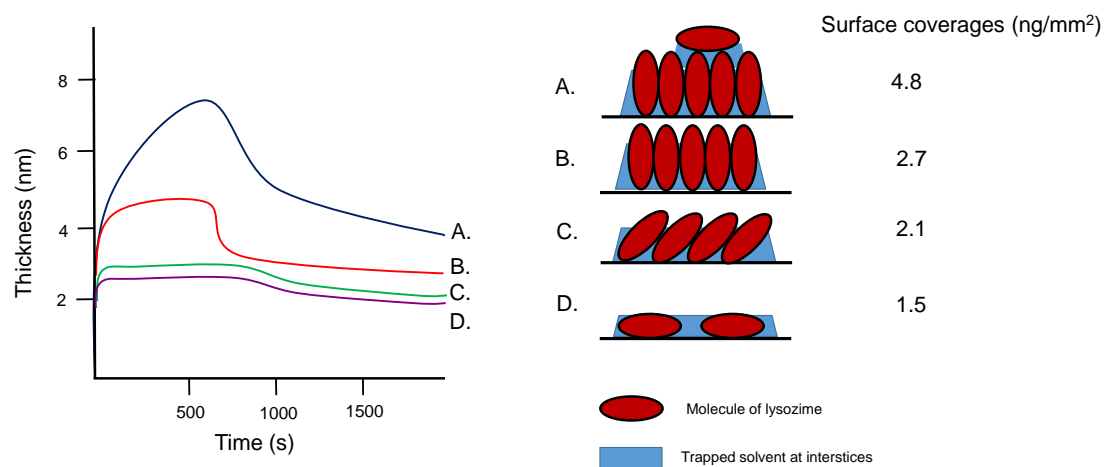


**Figure 14.** Orientations of lysozyme molecules according to the surface coverage.

Another study combining DPI and QCM-D was performed by Ash *et al.* in 2013 to investigate the *in vitro* generation of the salivary pellicle directly on the sensing surface.<sup>97</sup> The observed results suggested that Ca<sup>2+</sup> easily diffuses through the pellicle, allowing Ca<sup>2+</sup> ions to be exchanged between the adsorbed pellicle and the saliva under

physiological conditions, which promotes the enamel mineralization. Surprisingly, it was found that mass and thickness of the pellicle did not depend on low concentrations, which showed its adaptability to different physiological and environmental conditions.

Very recently, Ash and coworkers have investigated the structural changes observed in pellicles generated from stimulated whole mouth saliva and parotid saliva.<sup>98</sup> For the first time, the generation and structure of these pellicles were observed by contacting mouth and parotid saliva with QCM-D and DPI. Subsequently, the parotid saliva pellicle formed a denser layer than mouth saliva pellicle, suggesting that the proteins present in parotid saliva were also responsible for the formation of the dense basal layer of the acquired enamel pellicle. However, proteins present in the mouth saliva were more likely to help the generation of the softer outer layer of the pellicle. The authors concluded that salivary composition had an important effect on the structure of the pellicle.

DPI allows the properties of adsorbed protein layers to be measured with high exactitude to obtain a comprehensive description of adsorption processes. To this end, Ouberaï and coworkers have recently used a combination of two biosensing techniques, DPI and QCM-D.<sup>99</sup> From this, they have been able to extract surface coverage values, layer structural parameters, water content and viscoelastic properties to examine the properties of protein layers formed at liquid/solid interfaces. Layer parameters were examined upon adsorption of proteins of varying size and structural properties, on surfaces with opposite polarity. They have shown that soft proteins with high molecular weight are highly influenced by the surface polarity, as they form a highly diffuse and hydrated layer on the hydrophilic silica surface as opposed to the denser, less hydrated

layer formed on a hydrophobic methylated surface. These layer properties are a result of different orientations and packing of the proteins. Thus, these data have revealed a trend in layer properties highlighting the importance of the interplay between protein and surface for the design of biomaterials.

#### **6.1.4. Interactions**

Protein-protein interactions are the basis of cellular behavior, making them interesting as therapeutic targets. Hence, with more dynamic information available, researchers' attention has recently shifted from static properties to dynamic properties of protein interaction networks. Thus, DPI has been mainly used to study three different types of interactions. The first one involves antibody interactions, the second one is based on the protein-protein interaction, whereas the third interaction considers the non-protein ligands.

##### **6.1.4.1. Antibody**

Biosensor specificity relies strongly on the properties of the immobilized detection element. The use of antibodies in biosensing has increased in the last years, due to their molecular selectivity and high affinity binding characteristics for a particular target. In an early DPI publication,<sup>31</sup> the technique was employed to elucidate the kinetics of interaction between C-reactive protein and a monoclonal antibody immobilized on an aminated chip. The obtained results allowed the determination of the dissociation constant (0.45  $\mu\text{M}$ ), having close agreement with ELISA data, but the determination of the binding stoichiometry was also possible with DPI.

In a similar study, spectroscopic ellipsometry, NR and DPI were employed to study the binding between prostate specific antigen (PSA) and antibody at the water/silica interface.<sup>100</sup> Zhao *et al.* observed that the antigen-antibody interaction was maximum when the surface density was around 1.5 mg/m<sup>2</sup>. This was due to the structural changes occurring at the interface, which involved the insertion of antigens within the antibody layer. In addition, further studies demonstrated that the immobilized antibody was stable and active for more than 4 months.

As an example of immune-like interactions, fragments of antibody have also been determined by a biosensor based on DPI using biotin tagged protein G, immobilized by means of the avidin-biotin linking, as a recognition layer.<sup>101</sup> The acquired DPI data showed that the binding characteristics of both non-specific and protein G layer depended on the cross-linker used in the biotin film. The biosensor achieved a limit of detection about 1.7 µg/mL, with a dynamic range covering two orders of magnitude. In addition, the correlation between the structure and the activity of each layer was established considering real-time measurements provided by DPI.

In 2012, the interaction between BSA and anti-BSA Immunoglobulin G (IgG) was studied.<sup>102</sup> In this work, the mathematical model proposed for the fitting of empirical results obtained by DPI was proposed and allowed the two binding BSA molecules to be located with regard to the antibody probe. It was established a further reorientation of the first Fab fragment after binding of BSA molecules by its polar axis due to steric hindrance (Figure 15). Thus, the second binding BSA suffered two consecutive orientation processes in order to be bound by the second Fab fragment through its equatorial axis. Furthermore, the simultaneous determination of the conformational dynamics allowed

establishing the importance of conformational selection and induced fit on the biomolecular recognition.

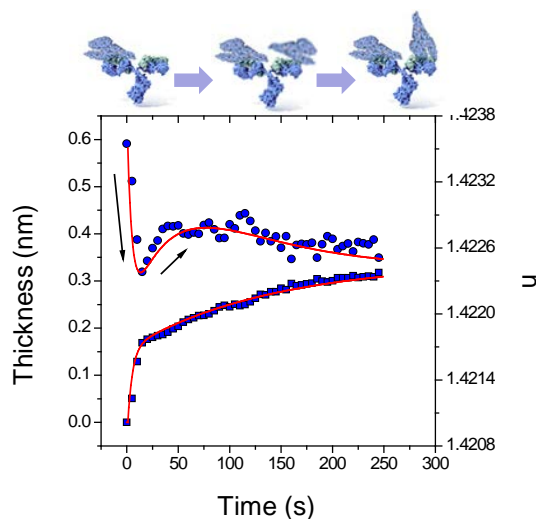


**Figure 15.** Proposed scheme of antibody-BSA interaction.

In 2012, Cowsill *et al.* assayed the key stages of the simplified human chorionic gonadotropin pregnancy test immunoassay.<sup>103</sup> Initially, anti-human chorionic gonadotropin antibody was adsorbed onto the bare SiON chip, followed by a blocking process with BSA so as to avoid the non-specific analyte adsorption, and finally human chorionic gonadotropin was bound to the antibody, the three steps monitored continuously. The authors observed that the higher amount of adsorbed antibody, the lower BSA co-adsorption, so that the global layer thickness was nearly constant, evidencing the filling of the gaps within the adsorbed antibody film with BSA molecules, which effectively minimized the non-specific adsorption.

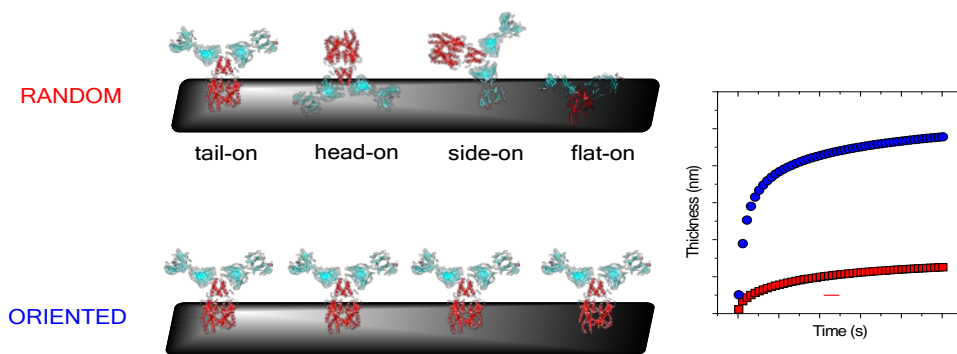


**Figure 16.** Antibody orientation on biosensor surfaces.

In the same year, a study dealing with the different orientations adopted by immobilized antibodies was performed using DPI and SPR was performed and different thickness data were measured (Figure 16).<sup>104</sup> For that purpose, thiol modified DPI chips were functionalized with sulfo-N-[ $\gamma$ -maleimidobutyryloxy]succinimide ester, and then, two strategies of immobilization were assayed: direct covalent binding and Fc-fragment binding to a protein G layer previously linked to the functionalized chip. The data showed that the first strategy led to a random orientation, whereas the second one resulted in an end-on orientation. The sensitivity achieved with oriented antibody surfaces (10 pg/mL) was suitable for clinic diagnosis (<30 pg/mL), whereas the randomly immobilized antibody surface could not detect even 1 ng/mL of the analyte. Furthermore, the authors concluded that DPI showed to be better than SPR for the unambiguous detection of antibodies.

Recently, a DPI assay was also used to measure the interaction of a copolymer immobilised on the chip with antibodies acting as mimic of the allergen-reactive immunoglobulin E.<sup>105</sup> The contribution from specific and non-specific binding was assayed from total serum protein containing immunoglobulins G and E. The antibody response was further tested using streptavidin-conjugated quantum dots, showing long

term stability and non-fouling properties of the coating, and very little specific binding with responses below 0.84 ng/mL. The quantum dot attachment could be observed as a change in contrast due to optical absorption and also used the measured quantum dot layer thickness (which was in agreement with the manufacturer specified dimensions) and refractive index, to derive an estimated molecular weight for the nanoparticle, as commented above.

#### **6.1.4.2. Protein ligand**

Proteins are frequently used as conventional drugs for the treatment and prevention of diseases.<sup>106</sup> However, the underlying intrinsic biochemical mechanisms for these substances remain still unclear in many cases. Due to its special characteristics, DPI has significant utility in the analysis of protein interactions.

In an early publication, Swann *et al.* established the conformational changes that take place during the streptavidin-D-biotin binding (Figure 17).<sup>73</sup> The authors observed that the film thickness increased around 6.6 nm when the streptavidin was immobilized, which is in agreement with X-ray crystallographic data (long axis of the apo-core-streptavidin molecule around 6.8 nm). Therefore results suggested the generation of a monolayer of immobilized protein on the surface. Interestingly, streptavidin was displaced from the surface as a result of the higher affinity exhibited for free than for immobilized D-biotin. Furthermore, the biotin layer was solvated and “inflated”. It was also established that there is a ratio between the likely (specific) molecular interactions and the densification of the protein film. This one provided a higher selectivity for label-free molecular systems.

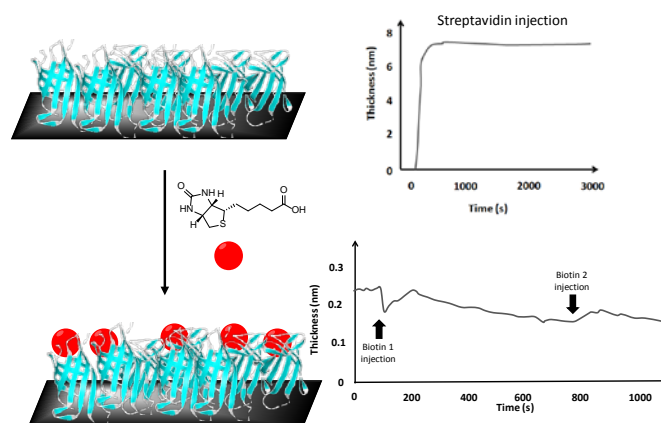


**Figure 17.** Monitoring the conformational change in the streptavidin-D-biotin binding.

In 2004, the specific interactions of the isoforms of Apolipoprotein E (Apo E) with tissue plasminogen activator (tPA) were investigated by CD and DPI.<sup>107</sup> In this study, the activator was anchored to amine chips via the bisulfosuccinimidyl suberate chemistry, and the Apolipoprotein isoforms were allowed to bind it. It was observed that Apolipoprotein E2 interaction with immobilized tissue plasminogen activator led to important conformational changes not detected with Apolipoproteins E3 and E4. The authors concluded that these interactions were involved in the mechanism of modulation of tPA's proteolytic activity by Apo E, which resulted in altered proteolytic and thrombolytic degradation.

In another work, the  $\lambda$  phage protein ( $\lambda$ O) interaction with a hydrophobic area on the larger surface of the dimer of a zinc-binding domain in the protease ClpX was also studied.<sup>108</sup> From mass data, it was deduced that two  $\lambda$ O molecules bound each protease, in a mechanism with two independent binding events: the first  $\lambda$ O bound weakly, whereas the binding of the second  $\lambda$ O was dramatically favored by the presence of the first protein.

The interaction between enolase from *Streptococcus pyogenes* and canine plasminogen has been investigated by means of DPI in a very recent publication.<sup>109</sup> Plasminogen is a monomeric protein constituted by seven independent domains established into a lock washer, which binds to enolase. However, both biomolecules are not bound in solution. Kornblatt and coworkers have demonstrated that the binding of *Streptococcus* enolase to the surface was an essential requirement for the formation of stable complexes between both native proteins. Hence, enolase-attractive surfaces are an indispensable requirement for binding plasminogen.

Protein assembly phenomena is also a potential field where DPI can be very useful, and several applications can be found in this area. E.g. Daghestani *et al.* studied the growth of tubulin microtubules on the surface and the effect of stabilizers and destabilizers.<sup>110</sup> For the immobilization of tubulin on commercial amine chips, the employed reagent sequence was NHS-biotin, streptavidin and finally biotinylated tubulin. By flowing tubulin in solution over the final surface, a net final increase in mass and thickness around 5 ng/mm<sup>2</sup> and 22.7 nm, respectively, was recorded, as well as a continuous decrease in density around 0.17 g/mL, which evidenced the formation of hollow vertical microtubules on the surface. The continuous register of the three parameters indicated that first protein protofilaments were formed and elongated, and after 10 min protofilaments joined together laterally to form the microtubule (Figure 18).

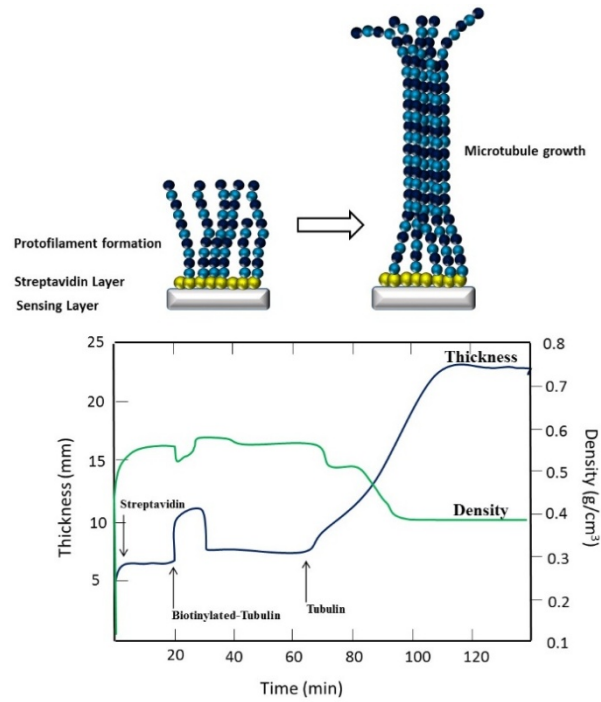


**Figure 18.** Characterization of the microtubules growth.

A practical application was reported by Zhai *et al.* for the real-time monitoring of amyloid  $\beta$  peptide aggregation and fibril formation.<sup>111</sup> The most relevant peptides (namely A $\beta$ 40 and A $\beta$ 42) were adsorbed on two different chips: a hydrophilic unmodified SiON and a hydrophobic C18 functionalized surface. The results showed that peptides adsorbed on silicon oxynitride did not aggregate, while hydrophobic C18 surface triggers the amyloid  $\beta$  aggregation process and served as a template for amyloid fibril and peptide self-assembly generation (Figure 19). The whole process began by the self-assembling of immobilized peptides and generation of the critical nucleus for amyloidosis, which produced in a density decrease with no significant changes in mass, and further association of the peptides in solution (that can also be in form of protofibrils or fibrils) with the immobilized nucleus.

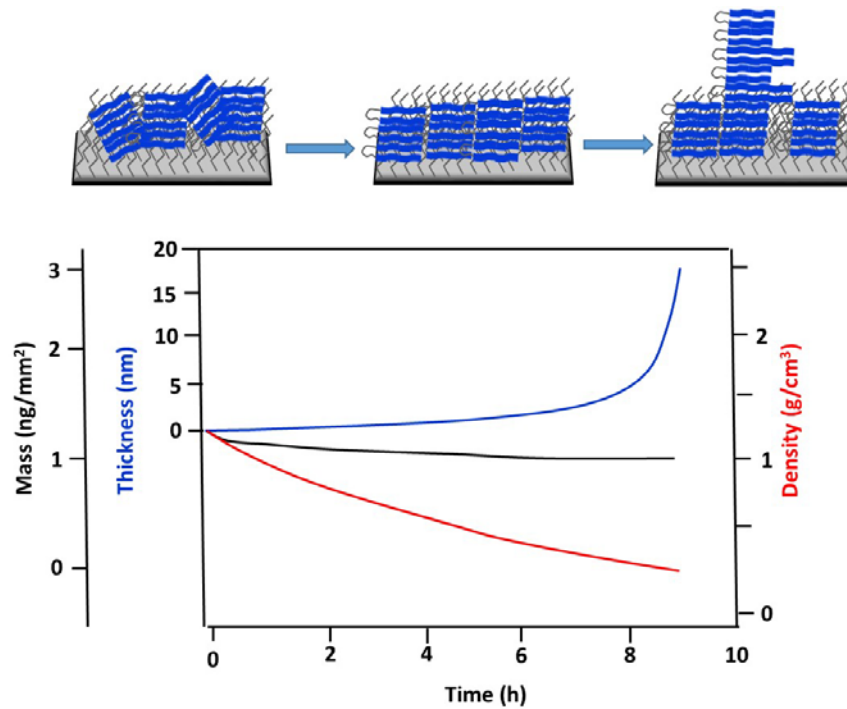


**Figure 19.** Schematic representation of the amyloid  $\beta$  aggregation process on the C18 chip.

Another related research performed by Gupta *et al.* was based on the knowledge of the disruption mechanism of fibrils formed by the serum protein transthyretin, using biphenyl ethers.<sup>112</sup> Initially, transthyretin was adsorbed on the chip, and the first stage of fibrillation showed a decrease in density ( $-0.05 \text{ ng/mm}^3$ ) and an increase in thickness ( $+1.3 \text{ nm}$ ) and mass ( $+0.77 \text{ ng/mm}^2$ ). On the contrary, in the presence of the inhibitor, no fibrillation happened, which was deduced by an increase in density ( $+0.17 \text{ ng/mm}^3$ ) and a decrease in thickness ( $-0.82 \text{ nm}$ ) and mass ( $-0.15 \text{ ng/mm}^2$ ). The authors suggested that the protein was ideally adsorbed as a monolayer, which led to the formation of oligomers and fibers after the subsequent protein deposition.

In this line, DPI was also employed to follow the real-time  $\alpha$ -synuclein aggregation that take place in a solution of molecular chaperone  $\alpha\beta$ -crystallin, which acted as an inhibitor of this process at its earliest stages.<sup>113</sup> Thickness, mass and layer

density during four hours of fibril elongation were displayed in presence and absence of inhibitor. It was observed that thickness and mass increased while density decreased when fibrils were growing, but in presence of  $\alpha$ -crystallin, these three parameters remained constant. The authors concluded that the inhibition happened by binding to partially folded monomers, avoiding in this way their aggregation into fibrillar structures.

#### **6.1.4.3. Non-protein ligand**

Due to its special characteristics, DPI is particularly effective for the study of protein interactions, as it allowed the stoichiometric ratio to be reliably calculated for heparin and a recombinant fragment of collagen V.<sup>114</sup> Initially, a streptavidin film (surface density 2.105 ng/mm<sup>2</sup> and 92% coverage) was adsorbed on the sensing chip, which bound to 0.105 ng/mm<sup>2</sup> of biotinylated heparin (stoichiometric ratio of 1:6). Heparin was interestingly able to bind collagen (0.154 ng/mm<sup>2</sup>), the collagen–heparin complex being inserted into the streptavidin layer. Finally, a stoichiometric ratio around 1.7:1.0 was estimated for this complex, which can be hardly calculated by SPR.

Interestingly, Popplewell *et al.* developed an oligosaccharide-immobilization strategy to covalently attach sugars onto a hydrazide-functionalized surface for its oriented coupling.<sup>115,116</sup> DPI allowed the determination of sugars that were readily available for binding proteins. The structural parameters of protein-sugar complexes were studied, and new features of the tested biomolecules, lactoferrin and fibroblast growth factor, were revealed. The described results showed that lactoferrin adopts different orientations depending on protein loadings, whereas for the growth factor a single monolayer bound to the surface was observed.

Nowadays, there is a significant interest in the development of hydrogel-based molecularly imprinted polymers (HydroMIP) and their possible applications extend to either diagnostics or therapeutics.<sup>117</sup> In this regard, DPI has been efficiently used to characterize and develop HydroMIP-based protein biosensors.<sup>118</sup> Reddy *et al.* first demonstrated the integration of MIPs with DPI in the development of optical protein sensors based on synthetic receptors. A polyacrylamide-based molecularly imprinted polymer was developed to detect bovine hemoglobin. The binding between the polymer and the protein was performed in two different formats. In the first approximation, hemoglobin was adsorbed on the chip and selective imprinted polymer was able to strip-off it from the surface (thickness and mass decrease by more than 1 nm and 0.2 ng/mm<sup>2</sup>, respectively). In the second one, hemoglobin binding to polymer-coated chip was registered, resulting in an increase in mass by 0.5 ng/mm<sup>2</sup> but thickness nearly constant, which suggested that hemoglobin bound into cavities below the film surface.

Recently, Jiang and coworkers used DPI in combination with Fourier transform infrared spectroscopy (FTIR) and <sup>1</sup>H NMR to study the interaction between BSA and the gemini surfactant diglycol bis-*N*-tetradecyl nicotinate dibromide (EQ14-2-14).<sup>119</sup> The authors observed that the binding of the surfactant increased the mass and thickness of the BSA layer; on the contrary, density and refractive index initially increased and then leveled off. The results showed a reduction of  $\alpha$ -helix from 54 to 32 % with an increment in random structure from 8 to 22 %. These results revealed that the addition of the surfactant induces  $\alpha$ -helix decreasing,  $\beta$ -anti turn and random structure increasing, which was confirmed by molecular docking data.

In a parallel study, Arthur and coworkers studied a similar gemini surfactant glycol bis-N-tetradecyl nicotinate dibromide (P14-1-14),<sup>120</sup> observing that the surfactant quenched the intrinsic fluorescence of BSA by means of the formation of a BSA/surfactant complex (binding constant around  $2.14 \cdot 10^4$  L/mol). As well, the binding of surfactant diminished the contents of  $\alpha$ -helix (from 54.01% to 29.41%) and raised the random structure (from 7.86% to 22.27%). Thus, DPI was proven to be an effective tool to monitor the interaction between BSA and gemini surfactant.

## **6.2. DNA Studies**

### **6.2.1. Immobilization and hybridization events**

In the last decades, numerous optical techniques have been employed for the detection of DNA hybridization, namely, SPR, fluorescence, interferometry, chemiluminescence, UV spectroscopy, and surface-enhanced Raman scattering spectroscopy (SERS).<sup>121</sup> However, DPI detection provides more information on these systems than the above-commented techniques since several parameters can be simultaneously quantified.

In 2005, Berney and Oliver published a pioneering paper, in which DPI was used for the study of nucleic acid based interfaces.<sup>122</sup> They discovered that electrolyte concentration and adsorbed amount of ssDNA were inversely proportional. On the other hand, the amount of biotinylated duplex DNA captured by an avidin film is four times fewer than that observed when duplex DNA was bound by means of an amine end terminal. Moreover, when probe concentration was increased from 0.1  $\mu$ M to 1  $\mu$ M, the

thickness increment was 10-fold faster and as a result, the close grafting density obtained resulted in unavailable probes for hybridization.

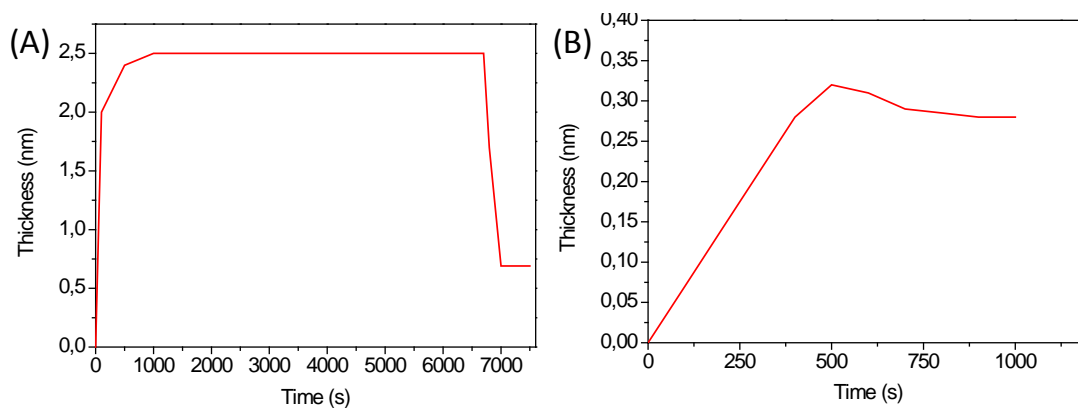


**Figure 20.** Measured changes in thickness values after probe layer formation (A) and hybridization detection (B).

A year later, Sheehan and coworkers studied the ability of DPI to characterize the ssDNA covalent immobilization and monitor selectively the target DNA hybridization on a silanized chip.<sup>123</sup> Probe coverage and its orientation were determined in real-time at the different steps of the immobilization process. From the experimental data, an increase of thickness of 0.69 nm was measured after probe layer formation (Figure 20.A), which suggested a flattened attachment to the surface. Interestingly, the small increase observed upon addition of the complementary target (0.28 nm) indicated that the orientation of probe film did not change significantly after hybridization (Figure 20.B). Furthermore, the effect of probe mobility on hybridization was also elucidated.

Lu and coworkers studied the DNA physical adsorption onto cationic diblock copolymers containing phosphorylcholine groups by combination of different techniques, such as spectroscopic ellipsometry, NR and DPI.<sup>124</sup> Thus, the DNA surface density

depended on the amount of preadsorbed cationic copolymer, which could be controlled by the pH. The authors concluded that the structure and size of DNA affected the intermixing and the surface layer and charge distribution.

In 2009, Kato *et al.* investigated the effect of salt on the growth and stability of a polyelectrolyte multilayer comprised of two different block sequences of DNA and polyethyleneimine.<sup>125</sup> The thickness and mass data showed a dependence between the layer growth and the sequence of the oligonucleotide. Consequently, the layer growth was modeled, which allowed DNA multilayers films, with the desired thickness, density and stability, to be molecularly designed.

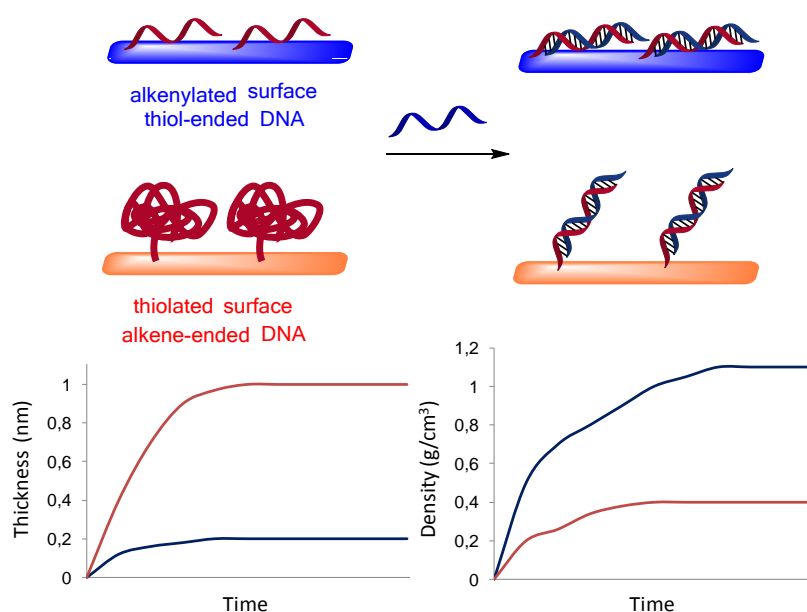


**Figure 21.** Hybridization model based on DPI measurements.

The immobilization of DNA probes onto different functionalized surfaces has also been investigated by several authors. An immobilization study of aminated DNA probes onto an ICPTS-silanzed surface was monitored online, estimating probe coverages of 1.8

·  $10^{11}$  molecules/mm<sup>2</sup>, which corresponds to a surface coverage around 10%. When hybridization events were monitored, efficiencies around 43% were estimated by means of the change in mass after addition of target DNA.<sup>126</sup> Alternatively, a thiolated oligonucleotide was covalently immobilized onto a GOPTS-functionalized surface by UV photoactivation and hybridization was monitored.<sup>127</sup>

DPI in combination with ellipsometry has been successfully applied to study hybridization events in microarrays fabricated by the emerging thiol-ene reaction. Recently, Maquieira's group studied two different immobilization strategies based on this "click" reaction and the measured values were used to explain different hybridization phenomena (Figure 21).<sup>71</sup> In one case, experimental results revealed that attached probe lied flat on the surface, and consequently hybridization occurs horizontally, as confirmed by ellipsometry measurements, reporting a thickness increase around 1.9 nm after hybridization. For another case, the data of film thickness increase (around one nanometer) for the alkene probe were consistent with a Gaussian coil type immobilization. It is remarkable that DPI and ellipsometry showed a significant increase in layer thickness (9.5 nm) after hybridization, revealing that the coil was straightened out.

Very recently, Huang and Liang studied the adsorption of DNA with some cationic complexes ( $\text{Ca}^{2+}$ ,  $\text{Cu}^{2+}$  and  $\text{Co}^{3+}$ ) on bare and aminated silicon chip surfaces.<sup>128</sup> The results showed that the multiphasic adsorption observed could be due to either the geometric resistance or the electrostatic repulsion between complexes. In a similar study, they reported a DNA strand displacement from a double-stranded DNA in real-time.<sup>129</sup>

Liang and coworkers also investigated DNA hybridization chain reactions at solid-liquid interfaces at various salt concentrations.<sup>130</sup> They observed that the presence of Na<sup>+</sup> ions effectively counteracted the negative charge of the DNA chains, resulting in greater numbers of immobilized initiator ssDNA strands upon increasing the concentration of NaCl. At low salt concentrations, the ssDNA strands were attached uniformly onto the chip surface and extended into the solution due to the electrostatic repulsion between chains.

### **6.2.2. Interactions with small molecules**

The measurement of interaction of biomolecules with small compounds (under 1000 Da) is an area of increasing interest, especially in drug discovery. Interactions with metallic ions have been widely investigated as many biomolecular systems are influenced by cation concentration. In these complex systems, the mass changes are often significantly small and difficult to detect, but structural changes are more significant. In this regard, the use of DPI is of great interest for the small molecules sensing. Thus, various small molecules have been targeted by DPI based biosensors in recent years (Figure 22).

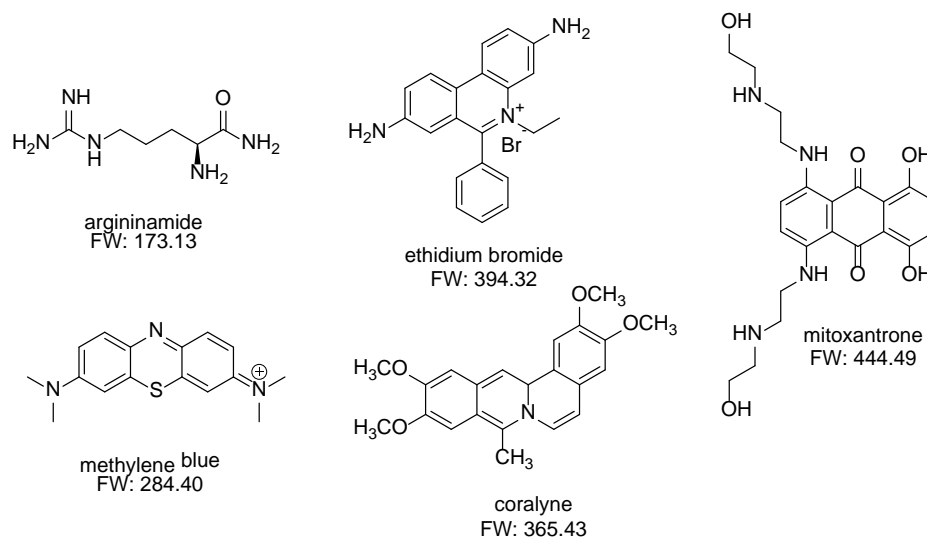


**Figure 22.** Small molecules detected through DPI based biosensors.

Yang and coworkers have demonstrated the application of DPI to study the binding between adenine-rich ssDNA and small molecules, for sensitive, direct and selective, and label-free, detection. In 2009, they described how the density and thickness of a ssDNA probe attached to a positively charged polyethylenimine adsorbed onto a silicon oxynitride surface changed in the presence of EtBr (ethidium bromide) and spermine, natural polyamine used to stabilize the DNA structure.<sup>131</sup> Interestingly, ssDNA was slowly contracted when EtBr was intercalated. Nevertheless, that intercalation and electrostatic interactions led to a slight increase in thickness together with a smaller increase in layer density of denatured DNA. In contrast, spermine led in all cases to a fast increase of thickness due to electrostatic interactions. In another work, these authors could effectively determine that the binding constants of mitoxantrone and methylene blue with DNA from the calculus of optical masses, obtaining values of  $1.8 \cdot 10^5$  and  $4.2 \cdot 10^4 \text{ M}^{-1}$ , respectively.<sup>132</sup>

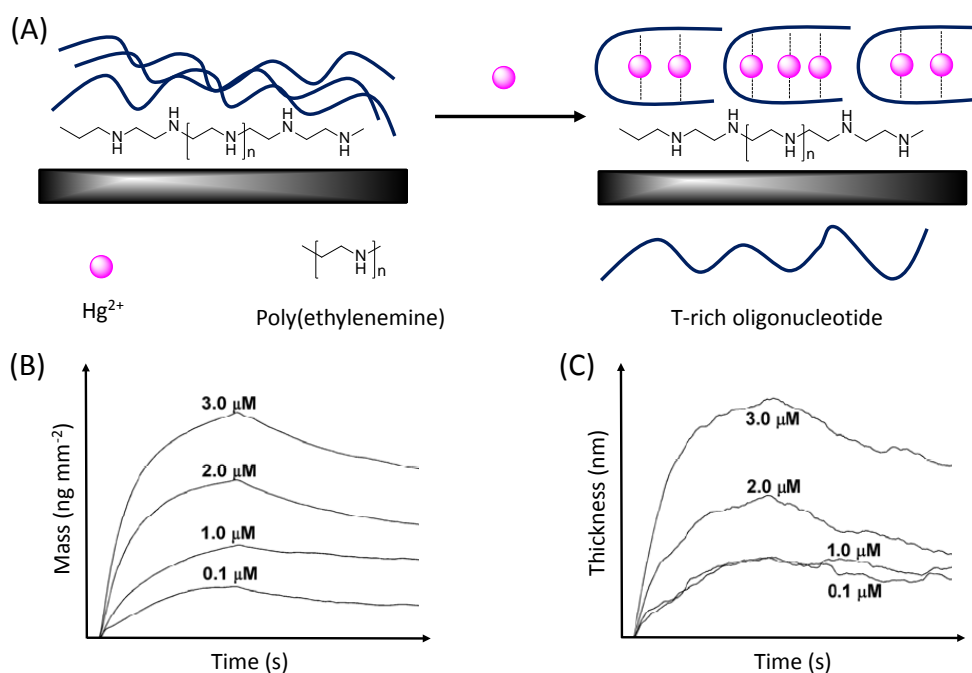


**Figure 23.** (A) Scheme of a Hg<sup>2+</sup> biosensor based on thymine–Hg<sup>2+</sup>–thymine coordination chemistry by immobilization of the probe onto poly(ethylenimine). (B) Mass and (C) thickness values after Hg (II) coordination.

The detection of a highly toxic heavy metal ion, such as Hg<sup>2+</sup>, has been reported by Wang *et al.*, who interestingly studied the interaction of a thymine(Thy)-rich oligonucleotide and Hg<sup>2+</sup>. Biosensing was based on Thy–Hg<sup>2+</sup>–Thy coordination chemistry. To this end, the probe was immobilized onto the poly(ethylenimine) electrostatically assembled on a bare SiON chip.<sup>133</sup> An increment in surface density and thickness was observed after addition of Hg<sup>2+</sup>, being due to the structural change of the probe from random coil to hairpin-like conformation (Figure 23). The detection limit was estimated to be 27000 μM, being under the toxicity level of this cation in drinking water (30000 μM). In addition, a high selectivity was also achieved because of the specific affinity of Thy towards Hg<sup>2+</sup>.

Wang's group also demonstrated the potential of DPI to study the biointeraction between an adenine-rich ssDNA and small molecules (such as coralyne).<sup>134</sup> They constructed a highly selective biosensor based on a negatively charged ssDNA adsorbed onto a preadsorbed poly(ethylenimine) layer on a silicon oxynitride surface. The 48-mer homoadenine ssDNA exhibited a high affinity for coralyne, while the homothymine control probe had no recognition. In addition, this method had a linear dynamic range between 12 and 0.5  $\mu\text{M}$  with a detection limit around 0.2  $\mu\text{M}$ .

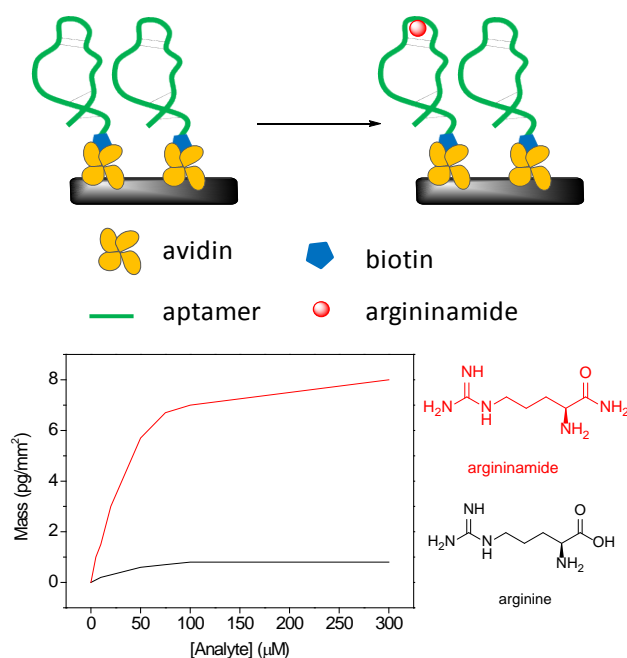


**Figure 24.** Schematic representation of argininamide binding and mass change after analyte injection.

Also in 2012, Özalp used this technique to quantify argininamide concentration using attached aptamers through the biotin-avidin interaction.<sup>135</sup> Initially, the layer thickness increased rapidly due the avidin immobilization, in agreement with its size. After injecting biotinylated arginine-aptamers, the thickness increased and the amount of aptamers deposited on the surface was found to be 0.077 pmol/mm<sup>2</sup>. From the results, a ratio of 2 biotin molecules was estimated to be occupying the binding sites of each avidin

molecule. The subsequent injection of argininamide caused a mass increase due to the formation of the aptamer-argininamide complex, and mechanical and structural changes were observed (Figure 24). The limit of detection of this biosensor was estimated around 5  $\mu\text{M}$  and the specificity was evaluated towards arginine, which was used as control analyte and as a result, insignificant changes in the deposited mass were observed.

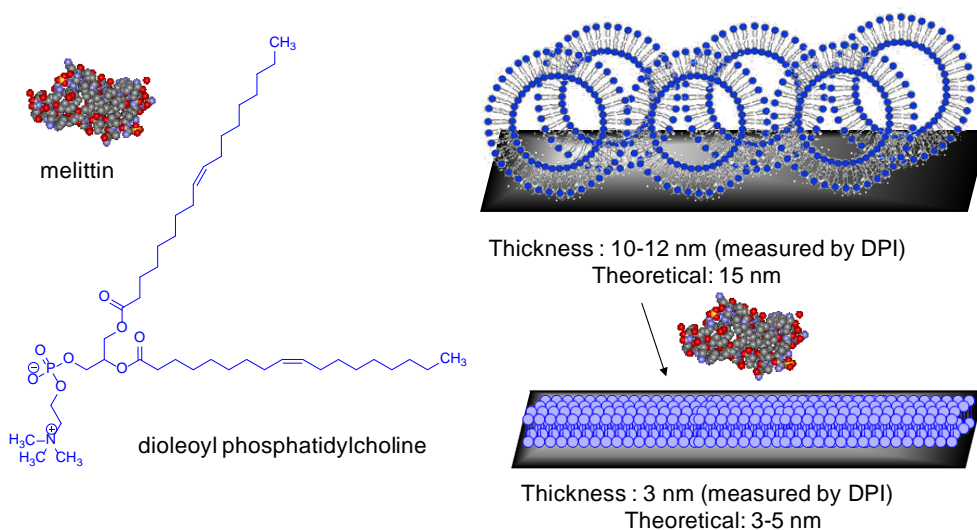


**Figure 25.** Schematic representation of lipid reorganization in the presence of melittin.

### 6.3. Lipid and membrane studies

DPI has been also increasingly applied to lipid and membrane physical studies. The structure, behavior and interactions of membrane and lipids are areas of active research, due to the current need to develop *in vitro* environments that mimic cell membranes.<sup>136</sup> The first application in this issue was reported in 2005 by Popplewell *et al.*<sup>137</sup> In this study, a dioleoylphosphatidylcholine liposome layers were deposited on the sensor chip, forming layers with 10-12 nm thick. Interestingly, when the liposome layer was challenged with the small protein melittin (26 amino acid residues), which is the main

toxin of bees, a dramatic rearrangement on the liposome layer was observed, giving a layer structure of 3 nm thick (Figure 25). The measured thickness decrease involved the formation of a planar lipid bilayer (3-5 nm thick). This work showed how real-time data on lipid structures and their behavior when challenged with peptides can be studied in detail using DPI.

In 2006, Terry *et al.* demonstrated the potential of this novel technique as it could efficiently difference in hybrid bilayer membranes formation and structure.<sup>138</sup> Thus, the results provided by DPI served to confirm the torridoyal model to quantify the effects of the melittin peptide on liposomes.<sup>139</sup>

Similarly, Khan *et al.* demonstrated that lipid redistribution occurred already in the adsorbing liposomes before the liposome-to-bilayer transition step.<sup>140</sup> DPI enabled sensitive determination of mechanistic details for the supported lipid bilayer formation in real-time, for which structural shifts and disposition took place.<sup>21,141</sup> Additionally, DPI data raised the possibility that a decline in tocopherol sensitivity gave rise to the functional defects observed in cell membranes associated with the severe ataxia with vitamin E deficiency phenotype.<sup>142</sup> Furthermore, DPI results strengthened the hypothesis that prion protein–lipid interactions are important in both the conversion and the pathogenesis of transmissible spongiform encephalopathies.<sup>143</sup>

In order to study the action of synthetic antimicrobial peptides (V4 and TV4) on model membranes, their interaction with solid supported lipid bilayers was investigated.<sup>144</sup> The results showed that V4 was inserted into the membrane after a preabsorption process. This effect was more evident at high V4 concentrations, where the

birefringence decreased sharply at the beginning and then increased slowly. The results probed that the lipid chains are aligned after the chronic disruption caused by V4 peptides. Interestingly, the results obtained for TV4, a truncated version of V4 used as control, indicated its binding but not its penetration into the membrane.

Later, Zwang *et al.* demonstrated that the DPI-QCM-D tandem allows the study of the hydration of supported lipid bilayers.<sup>28</sup> As a result, it was demonstrated that significant water uptake accompanied the antimicrobial peptide interactions with the membrane.<sup>145</sup> At this point, it is important to emphasize that water played a fundamental role in cell membrane structure in that it drove the formation of the lipid bilayer and that can be detected by DPI in real-time.

In 2010, Lee *et al.* reported the employment of DPI as biophysical tool to measure the membrane perturbation produced by antimicrobial peptides. The real-time measurement of the membrane-ordering properties in relation to the bound-peptide density,<sup>146</sup> led to a better knowledge of the interaction steps. In consequence, four different transitions were monitored during the action mechanism of those peptides<sup>147</sup>: (A) peptide binding to the film with insignificant effect on the membrane order, (B) peptides accumulation on the surface, (C) peptide insertion into the membrane and (D) membrane lysis via a detergent or micelle-like mechanism. In the same year, the generation of nonaggregated capsosomes composed of numerous liposome layers was also studied.<sup>148</sup>

A new approach to biorecognition, in which communication was regulated via the behavior of the collective lipid bilayer, was documented in 2011.<sup>149</sup> Membrane

cholesterol was able to induce a reduction in toxin binding to the glycan moieties of the receptor, tilting the head group. This function plays an important role in the activation of sperm fertility, indicating that the lipid-allosteric modulation regulates membrane recognition processes.

The potential of DPI for the analysis of complex conformational changes caused by peptide insertions into liquid-crystalline membranes has also been demonstrated.<sup>150</sup> It is worth emphasizing that with this platform the interaction of numerous proteins with a specific lipid head group can be so monitored in stable conditions, accordingly a different perspective on the time evolution of the interaction can be obtained.<sup>21,151</sup> The monitoring of the different binding steps allowed the time optimization for affinity analysis of this process. This result evidenced the ability of DPI for monitoring the supported lipid bilayer generation;<sup>141</sup> and it allowed confirming that the presence of these bilayers led to an efficient separation of biomolecules with better recoveries, given that their self-interactions decrease.<sup>152</sup>

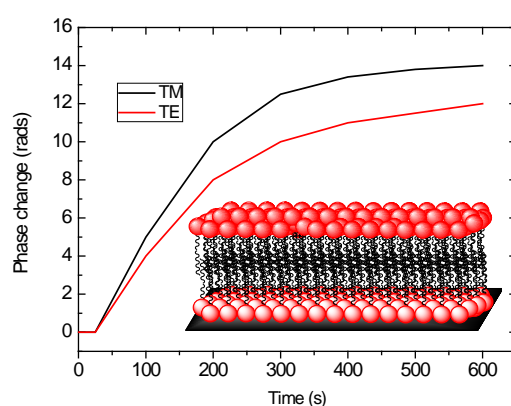


**Figure 26.** Monitoring of phase changes during the generation of supported lipid bilayers.

Figure 26 shows that TM and TE exhibited a hyperbolic dependence with time when lipid vesicles interact with SiON surface.<sup>152</sup> However, the profiles of birefringence for large unilamellar vesicles-forming supported lipid bilayers showed a gradual decrease in birefringence values. Considering previous results, it could be established that this transition to supported lipid bilayers took place in various stages: (A) vesicles adsorption on the SiON surface; (B) union of these lipid vesicles with neighboring vesicles; (C) formation of smaller lipid vesicles from larger ones; and (D) generation of a supported lipid bilayer.

On the other hand, Singh *et al.* demonstrated that peptides were incorporated into the membrane throughout the binding process of membrane and lipopolysaccharide.<sup>153</sup> Accordingly, the apoEdpL-W peptide could be inserted into the lipid membrane by three distinct stages.<sup>154</sup> Initially, the molecule was associated with the layer in a flat orientation, which caused the subsequent membrane disruption, and finally the dissociation of the peptide occurred (Figure 27).

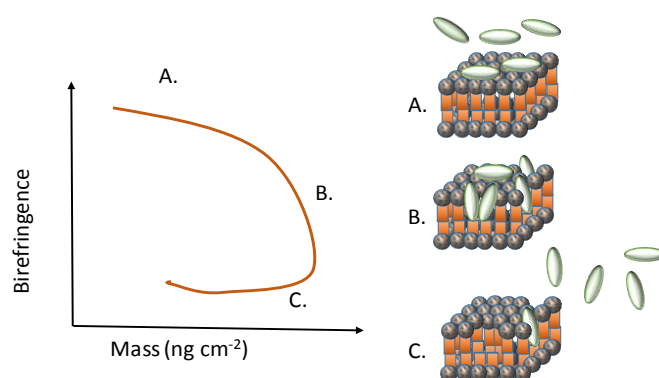


**Figure 27.** DPI analysis changes in birefringence associated with mass uptake of apoEdpL-W on a pre-formed lipid bilayer upon association with the bilayer (A), membrane disruption (B) and dissociation of the peptide (C).

Karst *et al.* applied this technique in the determination of the partition coefficient.<sup>155</sup> The DPI results were processed to quantify the partition coefficient and the binding kinetic parameters for the polypeptide AC489, ranging from  $5 \times 10^5$  to  $3 \times 10^4$  depending on the concentration tested. The decrease of partition coefficient when the protein concentration increased showed an anticooperative binding is anticooperative. From the results obtained, the transfer free energy from the buffer to the lipid phase could be also estimated between -6 and -8 kcal/mol.

As commented above, the changes in bilayer order can be examined in real-time by analyzing the dependence between the peptide mass bound to the bilayer and the birefringence of this film.<sup>156</sup> Thus, the ability to characterize each bilayer system in combination with NR allowed the accurate quantitative monitoring of the bilayer.<sup>24</sup> Consequently, it is possible to study changes in the membrane distribution during the peptide-membrane biointeraction, going into detail about the mode of interaction. In this regard, Singh *et al.* showed how peptide binding results in an essentially membrane disorganization with increasing peptide incorporation.<sup>157</sup> This research group also monitored interaction kinetics of bacterial lipopolysaccharides and peptide amphiphiles obtained from the human thrombin.<sup>158</sup>

AFM imaging in combination with DPI can clearly show how some membrane regions become thinner after removal of a portion of lipid molecules. Recently, Ouberaï *et al.* described the use of DPI in combination with *in situ* AFM to propose a model of interaction and explain the impact on the binding of membrane environment properties in terms of lipid composition (the lipid chemistry and steric properties) and bilayer structure.<sup>159</sup> Authors showed that the binding of  $\alpha$ -synuclein to membranes took place as

a result of the insertion of the biomolecule in head-group region, laterally expanding the lipid bilayer that induces a film remodeling and expansion of lipids outward the plane. That study provided insightful conclusions about the affinity of  $\alpha$ -synuclein for lipid packing defects.

Similarly, this tandem showed in 2013 that the antimicrobial peptide GL13K interacts with 1,2-dioleoylphosphatidylcholine planar bilayers. Thus, the DPI-AFM tandem demonstrated the existence of layer portions where some lipid molecules were eliminated by means of peptide-induced micellization.<sup>160</sup>

A curve fitting process is usually necessary for the analysis of peptide-membrane interactions. In the study reported by Hirst *et al.*<sup>161</sup> kinetic models were fit to the previously obtained data of birefringence and mass corresponding to the different steps involved in those interactions. It was the first time that a mass and a structural/conformational change were fit using the same kinetic model parameters. Very important information about the interaction could be quantitatively analyzed, and it was used for the description of the different intermediate states. Using this self-consistent method, the authors proposed a mechanism for the binding of the peptide to fluid state membranes including the roles of each state. According to it, in the first state peptides were loosely attached to the membrane with a high dissociation rate. During the second state, peptides were reorganized, which resulted in some membrane rearrangement. Lastly, in the third state a significant membrane disruption and membrane spreading was observed.

Finally, supported lipid bilayers shows great potential to study of membrane properties. In this regard, DPI can be also used as a scaffold for biosensing tools. For example, it is useful to study the alignment of both graphene oxide flakes and lipid molecules.<sup>162</sup> These studies have opened up a myriad of novel preparation procedures to intercalate structures (such as graphene or graphene oxide) in lipid membranes.

#### **6.4. Polymer and polyelectrolyte studies**

As commented above, DPI was firstly designed as a technique to monitor biomolecule structure, conformations, interactions and other biological systems. However, the applicability of this powerful technology was soon exported to control other chemical processes involving the formation of molecular layers. The formation of organic molecular layers (mainly polymers and polyelectrolytes) on the chip surface, as well as their interaction with other molecules, are perhaps the most popular non-biological applications of DPI.

##### **6.4.1. Single layer adsorption**

In 2010, Bijelic *et al.* investigated complex adsorption properties of bottle-brush polyelectrolytes, consisting on long poly(ethylene-oxide) side chains attached to a methacrylate backbone.<sup>163</sup> Different sized bottle-brush polyelectrolytes, with a distinct ratio between non-charged poly(ethylene-oxide) side chains and unchanging cationic charged segments, were dissolved in water, then physisorbed on the chip and further desorbed by salt addition. The authors observed that the side-chain surface interactions increased as a result of the orientation adopted by the backbone of the non-charged polymers. However, for highly charged polymers, the layer became thicker as side chains

expanded away from the surface (Figure 28). They concluded that more expanded layers were formed at intermediate charge densities, which was due to the preferential accumulation of charged segments. When dilute solutions (100 mg/L) were used, the adsorption kinetics were relatively fast (tens to hundreds of seconds). These effects find important applications in the synthesis of biological polymers carrying different segments.

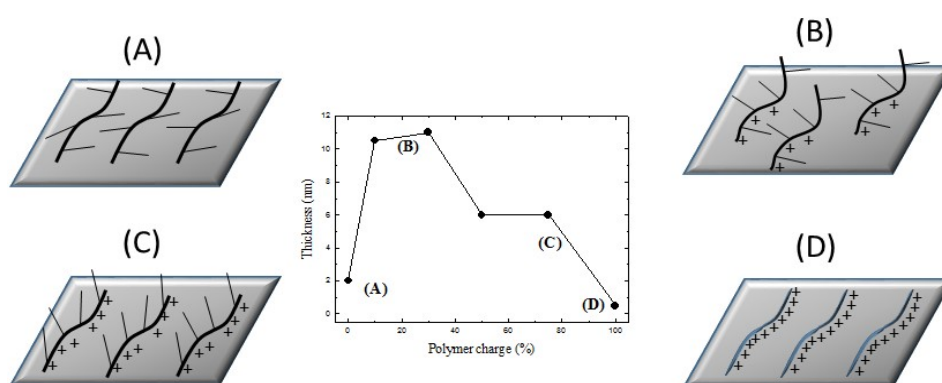


**Figure 28.** Adsorption of bottle-brush polyelectrolytes.

The same authors performed later combined DPI/XPS studies of adsorption of polyelectrolyte complexes.<sup>164,165</sup> In these studies, polyanion was poly(sodium styrenesulfonate), and two bottle-brush copolymers, with a distinct molar ratio between the cationic and nonionic segments, were employed as polycations. Polyelectrolyte complexes made by combining anions and cations were injected on the DPI chip surface and thus, their structural parameters (e.g. refractive index, thickness and surface density) were monitored in real-time. Complexes adsorbed on SiON were achieved when small amounts of poly(sodium styrenesulfonate) were present in the complexes.

In a simultaneous research performed by the same group,<sup>166</sup> cationic diblock copolymers poly(N-isopropylacrylamide)-*b*-poly((3-acrylamidopropyl)trimethylammonium chloride)<sub>x</sub> ( $x = 0, 6, 10, 14, \text{ and } 20$ ), were generated, and their adsorption onto SiON was studied. The lattice mean-field theory allows the polymer adsorption to be modeled. Both theoretical and experimental results showed that this phenomenon was conditioned by either steric hindrance or electrostatic interactions, depending on the ratio between polymers. Hence, it was established that at the beginning, the adsorption rate was limited by the mass transfer rate to the surface, whereas the attachment rate was the limiting factor for the adsorption when higher coverages were achieved.

Finally, a recent publication by Lu and coworkers showed a theoretical-practical report on the deposition of thin heterogeneous films and its measurement by means of DPI and ellipsometry, which usually employs a homogeneous single film model for the thin layers analysis.<sup>17</sup> In this study, new analytic formulae were proposed, which allowed heterogeneous layers to be investigated and compared with the empirical data generated by means of a slab model. This model was applied to the analysis of the deposition of the polyethylenimine on silica, and related to QCM-D data. This enabled a (very sensible) graded density structure model to be applied to the data and so reconcile the measurements from the two techniques. The authors went on to conclude that more information about surface morphology could be extracted thanks to data of the mass of light-absorbing molecules, which could be used to remove the uncertainty related to the layer composition, especially when different molecules enter into competition for one binding site.

### 6.4.2. Layer-by-Layer deposition

A very common use of DPI, applied to polyelectrolyte chemistry, is the monitoring of layer-by-layer deposition of charged polymers, in general alternating negative and positive layers. As shown in Figure 29, the layer growth is directly registered, and thickness and density data evolution are very helpful for the final application of the polymer multilayer.

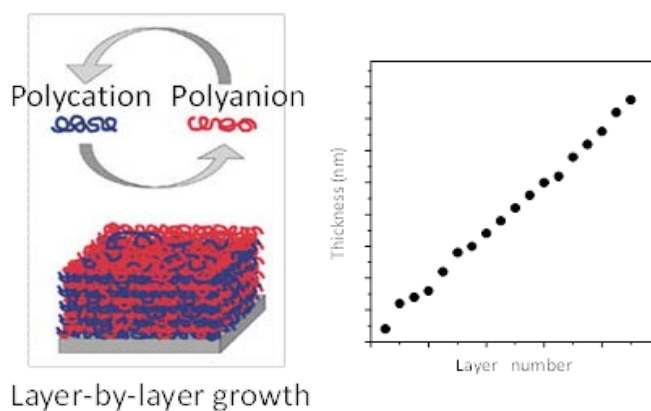


**Figure 29.** Thickness of layer-by-layer deposition measured by DPI.

In 2007, Edmonson *et al.* built a multilayer of two polymers, 20% 2-hydroxyethyl methacrylate and 80% 2-(dimethylamino)ethyl methacrylate as cationic copolymer and poly(glycerol monomethacrylate) as anionic one. The layer deposition was monitored by DPI and ellipsometry, achieving good agreement between both techniques.<sup>167,168</sup> Interestingly, interferometry data showed a linear trend of the increment of thickness (around 2.3 Å per layer), after 17 consecutive deposits. The final bromoester initiator density was around 4.9 groups nm<sup>-2</sup>, value comparable to that calculated by silane or thiol chemistry. The final multilayer was used as surface macroinitiator for synthesizing poly(2-hydroxyethyl methacrylate) via atom-transfer radical-polymerization.

Lane *et al.* employed DPI and QCM-D to study the multilayer formation of the polyanions poly(styrene sulfonate) and poly[1-[4[(3-carboxy-4-hydroxyphenylazo) benzenesulfonamido]-1,2-ethanediyl sodium salt], and the polycation poly(ethylenimine).<sup>169</sup> They observed that typically 5 or 10 layers of alternate polymers were built, always beginning by adsorbing the polycation on the unmodified chip. Surprisingly, DPI showed that multilayer formation was carried out in three steps. Firstly, polymer coils were adsorbed onto the surface, secondly they were flattened, and finally a transport into the film took place (Figure 30).

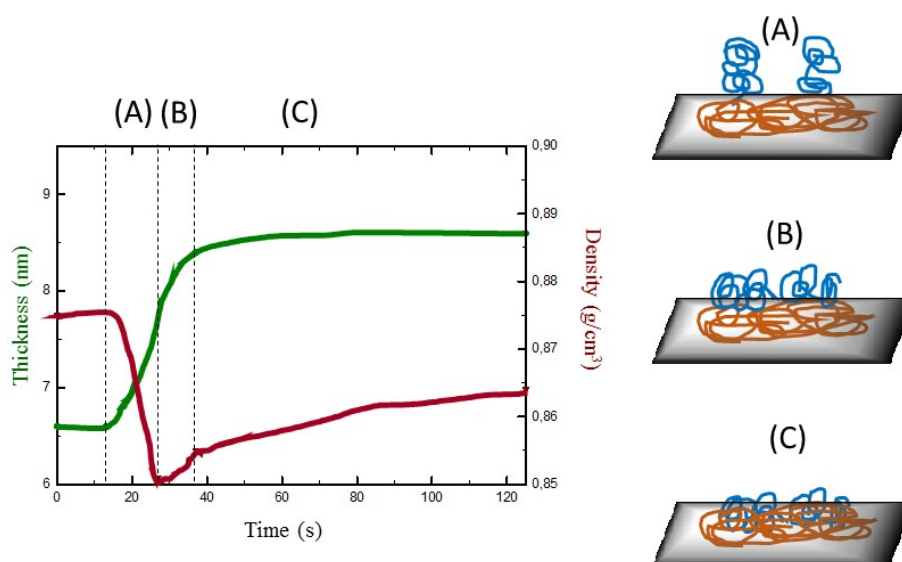


**Figure 30.** Schematic adsorption of a polyelectrolyte onto a complementary film.

In a different application, Aulin *et al.* used DPI and QCM-D to measure multilayers of polyethyleneimine and microfibrillated cellulose.<sup>170</sup> The results showed a regular accumulation of multilayers. Higher adsorption of polyethyleneimine, and consequently of cellulose, during the multilayer generation was observed for high values of electrolyte concentrations and pH. Nevertheless, the adsorption of cellulose onto polyethyleneimine was inhibited by an increase in the electrolyte concentration of the

cellulose dispersion. For the adsorption of 5 consecutive bilayers, starting with polyethyleneimine, it was found that the amount of both polymers was lower in the two first bilayers, but in the following ones, the adsorption was linear, the amount of cellulose being higher than that of polyethyleneimine. By combining the results from DPI and QCM-D, a total water content around 41 % in the multilayer was estimated.

In 2010, an interesting study was performed by Feldötö *et al.*<sup>171</sup> by combining DPI and QCM-D to monitor the structural changes of poly(allylamine hydrochloride)/poly(styrene sulfonate) multilayers and how it was affected by the rinsing agent. The authors concluded that poly(allylamine hydrochloride)-terminated layers rinsed with water, led to a swelling of the multilayer. The role of counterions on thickness was also studied. As a result, it was observed that thicker layers were obtained when using KBr instead of NaCl in the deposition solution.

Westwood and coworkers performed different studies using DPI, QCM-D and FTIR to investigate polymer multilayer properties of the anionic polygalacturonic acid. The first one was focused on the basic characterization of multilayers employing poly-L-lysine, chitosan, and lysozyme as polycations.<sup>30</sup> Multilayers of poly-L-lysine and chitosan polyelectrolytes showed a clear growth in thickness and mass during the deposition of the first 10 bilayers, but the lysozyme bilayers stopped growing after the fifth bilayer. A deep discussion about the deposition processes, taking into account thickness, refractive index and mass data, was carried out. Hydrated mass ratio (DPI compared to QCM-D) and polymer mass ratio (DPI compared to FTIR) were also discussed.

In a different work but employing the same polyelectrolytes, the role of the pH on the film stability was studied.<sup>172</sup> In order to study the reversibility of multilayer formation pH was first decreased (from 7.0 to 1.6) and later increased up to 7.0 again. As a result, the ten-layers film used to perform the study showed an irreversible thinning due to a partial disassembly. Loss of polycation was higher (50-80 % w/w) than that of polyanion (10-35 % w/w). The disassembly observed in the acid cycle was strongly dependent on polycation charge density, hence most of it took place at pHs lower than the pKa of polygalacturonic acid.

In 2011, a similar multilayer (polyethyleneimine and carboxymethylated cellulose nanofibrils) was studied with XPS, DPI, QCM-D and field emission scanning electron microscopy.<sup>173</sup> The results provided by QCM-D and DPI showed a rapid formation of the multilayer, in addition it was observed that cellulose layers were thicker than that of polyethyleneimine layers. The film growth was linear for the first deposited layers, but became nearly exponential towards the upper layers. In the first 5 bilayers, the average total water content was 56 %. Next, the mechanical properties of fibres used for paper sheets manufacture were evaluated performing depositions of polyethyleneimine/nanofibrillated cellulose, and polyallylamine hydrochloride/hyaluronic acid, on the surface of pulp fibres.<sup>174</sup> DPI showed that in the first system, thickness increased linearly with the number of layers and no dependence on salt concentration was observed, reaching approximately 20 nm thickness after 8 bilayers. In the second system, no linearity was shown, and films reached 27 nm after 5 bilayers. Furthermore, the surface treated with polyelectrolyte multilayers was shown to be highly stretchable.

Recently, the role of structure and molecular weight of poly-L-lysine on pH responsiveness of polygalacturonic acid-based multilayer films was tested.<sup>175</sup> The authors observed that when building the multilayer with low molecular weight linear poly-L-lysine (1 kDa), the loss of multilayer after pH cycling was nearly 90%, although much lower (50%) than that observed for heavier linear poly-L-lysine (200 kDa). Employing the dendrimer poly-L-lysine (22 kDa), the thickest multilayer was achieved, and nearly 60% polymer mass was lost and the film thickness decreased after the pH cycle.

Westwood and coworkers published a different study dealing with the effect of the activity of polygalacturonase on poly-L-lysine-polygalacturonic acid films, using DPI, QCM-D and AFM.<sup>176</sup> The results showed how an activity of 1 U/mL produced a fast (20 min) and almost complete destruction (more than 80 % of mass was lost) of the poly-L-lysine-polygalacturonic acid structure. However, for lowest activities, a negligible effect on poly-L-lysine-polygalacturonic acid films was observed. In addition, for multilayer films with poly-L-lysine uppermost a persistent delay was observed throughout the degradation.

On the other hand, Blomberg and coworkers monitored in 2011 the building of heparin (anionic) and polysaccharide multilayers of chitosan (cationic) by QCM-D and DPI.<sup>177</sup> They observed that chitosan was first adsorbed on the bare sensing surface, and then alternate layers of heparin and chitosan were laid on. Both mass and thickness showed an exponential increment with the number of layers, and the results were higher when solution had high NaCl content and a less pH. The molar ratio chitosan/heparine varied from 2.3 to 3.6, suggesting not only electrostatic interactions between chitosan and heparine but also short-range interactions, such as van der Waals forces.

In 2012, Johnson *et al.*<sup>178</sup> monitored the stability, structure and assembly of multilayers generated from mercaptoalkanoic acid films attached by thiol and carboxyl bindings with  $\text{Cu}^{2+}$  (Figure 31). They observed that addition of mercaptohexadecanoic acid to the previous layer increased thickness and decreased density, while when covering it with  $\text{Cu}^{2+}$  thickness decreased but density increased, due to an arrangement of the surface monolayer. The authors concluded that all those conformational changes were produced by electrostatic repulsions between adjacent  $\text{Cu}^{2+}$  ions. On the other hand, it was also observed that the oxidation state of those ions alternate between +2 when forming the copper carboxylate surface and +1 after the assembly of the adlayer.

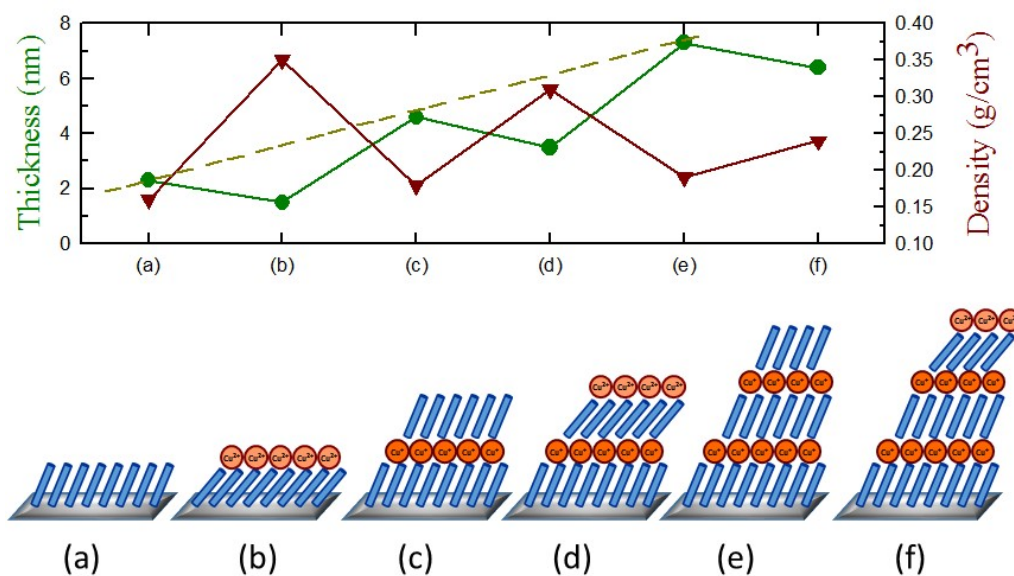


**Figure 31.** Monitoring a multilayer assembled from three mercaptoalkanoic acid films.

The monitoring of layer-by-layer deposition of polymers has not only interest *per se*, but also it has found a practical application in the fabrication of microcapsules, because the performances of the microcapsule walls can be established by measuring the properties of the polymer layers that walls are made of. In this regard, Becker *et al.*

fabricated in 2009 hydrogel capsules fabricated from disulfide cross-linked poly(methacrylic acid).<sup>179</sup> Capsules were fabricated on silica templates by layer-by-layer alternating thiol-functionalized poly(vinylpyrrolidone) and poly(methacrylic acid), cross-linking the thiol and further removing the poly(vinylpyrrolidone) and the templates. The process was also performed on QCM-D and DPI sensing surfaces, and thickness and mass of the polymer multilayer were recorded. Each thiol-functionalized poly(methacrylic acid) contributed to the film with 3.2 nm thickness and 2.1 mg/m<sup>2</sup> mass, whereas the poly(vinylpyrrolidone) layers caused increments of 1.6 nm and 1.4 mg/m<sup>2</sup>.

Facca *et al.* developed multilayered capsules made from poly-L-lysine and poly-L-glutamic acid, carriers of growth factors in bone formation.<sup>180</sup> Polyethyleneimine was the first layer coating the chip, and further alternate layers of poly-L-glutamic acid and poly-L-lysine were laid until a total of nine layers, the terminating layer being poly-L-lysine. Then, a bone morphogenetic protein (negatively charged) was adsorbed, followed again by poly-L-lysine and a further layer of transforming growth factor  $\beta$ 1. Thickness and surface density increased exponentially with the deposited layers, and the deposition of the morphogenetic protein and growth factor on the underlying poly-L-lysine layers resulted in an increment in both surface density and thickness, showing the successful insertion of negative proteins within the layers. The reported changes in thickness obtained after morphogenetic protein (3.4 nm) and growth factor (4.5 nm) adsorptions, were in good agreement with their reported dimensions, assuming that the proteins adopt a lateral or a “side-on” configuration. The mass densities were around 7.4 mg/m<sup>2</sup> and 5.2 mg/m<sup>2</sup> for growth factor and morphogenetic protein, respectively.

#### **6.4.3. Polymer interactions**

The research on polymer and polyelectrolyte surface chemistry goes beyond the monitoring of layer-by-layer deposition, because it can be expanded to interactions with other molecules or biomolecules. An early application of polyelectrolyte deposition as support for reagent immobilization was described in 2006 by Haltur *et al.*<sup>19</sup> The development of biodegradable poly(L-lysine) and poly(L-glutamic acid) multilayers on titanium or silica and the attachment of enamel matrix derivative protein, and its derivative, was studied by ellipsometry, QCM-D and DPI in real-time. It was observed that the successful attachment of the hydrophobic aggregating enamel protein both within and on top of the film structure at pH 5.0 was affected by the flow pattern during the process. The polypeptide-enamel matrix derivate protein multilayers are interesting due to their ability to induce biomineralization and trigger cell response.

The same year, Lord *et al.* applied DPI, QCM-D and SPR for monitoring the interaction of lysozyme with an acrylic-based hydrogel.<sup>181</sup> The combination of the three techniques showed that lysozyme, after initial absorption into the hydrogel matrix, displaced water in an amount higher than the absorbed protein. Microbalance data indicated that the displaced hydrodynamic water was greater than the gain mass of glycoside hydrolase monitored by DPI.

In 2009, Wang and Tam investigated the interaction of surfactants with polyelectrolyte grafted fullerenes.<sup>182</sup> At pH 6, the deposit of poly(2-(dimethylamino)ethyl methacrylate)(50)-block-C(60)) on the SiON chip resulted in a mass ( $\approx 0.5 \text{ ng/mm}^2$ ) and thickness ( $\approx 1 \text{ nm}$ ) increment, which agrees with the presence of the fullerene head. A further deposit of poly(acrylic acid)(83)-block-C(60) on poly(2-(dimethylamino)ethyl methacrylate)(50)-b-C(60) produced nearly the same increment in mass but lower (0.6

nm) in density, indicating a strong interaction between the two polymers, which was promoted by electrostatic attraction between negatively and positively charged segments. However, if the second negative layer was a double tagged C60- poly(acrylic acid)(83)-C60, the mass was lower than for the single-tagged one.

Furthermore, the same authors examined the adsorption of two non-ionic surfactants -TX100 (octyl phenol ethoxylate) and Brij 76 (polyoxyethylene 9 lauryl ether) - on the adsorbed poly(2-(dimethylamino)ethyl methacrylate)(50)-block-C(60)) layer.<sup>182</sup> Both surfactant interacted with the poly(2-(dimethylamino)ethyl methacrylate)(50)-block-C(60)) layer. For the ethoxylate, the binding occurred by means of pi-pi interactions between the phenyl ring of the TX100 and the C(60) head group.

The binding of surfactants to polyelectrolytes was studied by Varga *et al.* by deposition of consecutive films of sodium dodecyl sulfate and poly(ethylene imine).<sup>183</sup> The authors found that the structure of the preadsorbed poly(ethylene imine) layer had an important effect on the poly(ethylene imine)/surfactant interaction. Surprisingly, when the outer part of the layer contained a sufficient amount of polymer segments, desorption of poly(ethylene imine) could be prevented.

In a different approach, the activity of an immobilized antibody was aimed to be enhanced by anchoring the immunoglobulin on a polyelectrolyte multilayer.<sup>184</sup> The sensor surfaces of DPI and QCM-D were coated by a first layer of poly(ethylene imine) and further alternate layers of negative poly(Na-styrene sulfonate) and positive poly(allylamine-HCl) were deposited. The multilayer assembly was linear and the values obtained after five bilayers formation for water content (20-25%) and layer refractive

index (around 1.5) suggested a compact and rigid internal structure. Finally, the antibody probe was adsorbed on the multilayer, on both poly(Na-styrene sulfonate) and poly(allylamine-HCl), IgG being adsorbed more to poly(allylamine-HCl) terminated layers. Also, the antibody was sandwiched between polyelectrolyte layers, but its recognition ability was not better than when polystyrene supports were used.

The tandem DPI/QCM-D has been recently applied to an interesting study about the adsorption of fibrinogen on surfaces coated with different poly(ethylene glycol) chains (Mw 1000, 2000 and 5000).<sup>185</sup> It was demonstrated that on QCM-D chips, polymer tight chains were in extended brush conformations, while on DPI chips, the two light chains collapsed to a pancake-like conformation but the heaviest one (5000) had a mushroom conformation. Fibrinogen completely extended on the relatively dense poly(ethylene glycol) 1000-modified DPI surface (0.10 chains/nm<sup>2</sup>), but only partly on the poly(ethylene glycol) 2000-modified DPI surface (0.05chains/nm<sup>2</sup>), and did not adsorb on the deformable and mushroom-shaped, poly(ethylene glycol) 5000. Hence, the authors concluded that fibrinogen adsorption resistance of poly(ethylene glycol) surface depended on the deformation capacity of polymer interlayers and on its grafting density.

## **6.5. Functional Surface Characterization**

The characterization of functional surfaces is an important requirement for developing new materials in all biotechnological fields. In addition, the surface chemistry is helpful for the achievement of a deeper understanding of the interaction between the interface and the environment. Thus, DPI data are being used for it is assay development and/or understanding assays for ultimate use on other devices. The first manuscript on this issue

was published in 2008, using DPI for comparing modelled and experimental behaviour of C18 surfaces used in High Pressure Liquid Chromatography.<sup>186</sup> Results of thickness of linker-C18 on silicon-water (around 1 nm) and silicon-acetonitrile (around 4.3 nm) surfaces were in agreement with those obtained by theoretical HyperChem models.

Volcke *et al.* used DPI as a surface characterization technique in 2010 for the characterization of plasma coated surfaces.<sup>187</sup> 3-aminopropyltriethoxysilane was coated onto AFM tips, as well as silicon plates, by means of a plasma-enhanced chemical vapor deposition. DPI showed that coatings underwent a small growth when they come into contact with Tween, which involved an increment of thickness from 5.12 to 6.39 nm, keeping the (3-aminopropyl)triethoxysilane (APTES) mass around 3.80 ng/mm<sup>2</sup>. The surface density of amino groups was calculated about  $17 \cdot 10^{14}$  per cm<sup>2</sup>.

The same methodology was applied to derivatize a cyclo olefin copolymer surface with APTES to achieve a surface functional group.<sup>188</sup> For this, two time conditions were applied, with different results. The short one (30 s plasma) gave the same results as the previous reference (surfactant treatment increased layer thickness from 5.12 to 6.39 nm, and the APTES mass kept constant around 3.80 ng/mm<sup>2</sup>). However, a longer treatment (4 min plasma) led to a surface showing very small growth when in contact with buffer (thickness increased from 29.95 to 30.03 nm), and a drop of APTES mass film from 17.7 to 15.1 ng/mm<sup>2</sup> when it was washed with Tween. In a further paper from the same research team, the cyclo olefin copolymer was coated with different silanes for biochemical probe immobilization.<sup>189</sup> DPI showed that the number of surface amine groups was nearly  $78 \cdot 10^{14}$  cm<sup>-2</sup>, and treatment with buffer containing Tween diminished it until to  $66 \cdot 10^{14}$  cm<sup>-2</sup>.

DPI helped in the design of a sensor array of optical slot-waveguide ring resonators.<sup>190</sup> The sensing surface was coated with an anti-BSA antibody using glutaraldehyde as cross-linker. The same procedure was exactly carried out on the chip surface, as well as to estimate the immunoglobulin loading on the ring resonator surface assuming a reproducible procedure. The anti-BSA monolayer load was 2.0 ng/mm<sup>2</sup>. These results were successfully reproduced on slot-waveguide, avoiding a hard, laborious and costly work for developing biophotonic devices. Thus and as has been seen in previous examples, DPI data are being used for understanding assays for ultimate use on other devices.

## **6.6. Other Applications**

As described above, DPI presents a wide variety of applications in biophysics, drug research, surface science, biotechnology and lipid studies. However, it has also other uses that were originally developed to solve problems in other fields of research. Thus, Tan and Cross characterized the formation of an oriented monolayer of liquid crystal molecules of 4-n-pentyl-4'-cyanobiphenyl onto the chip surface.<sup>191</sup> It occurred in two steps: Firstly, molecules laid prone on the surface, and secondly, those molecules condensed and aligned leading to an increase in thickness of 1.66 nm with a molecular axis polar angle around 56°. It is worth mentioning that crystal molecules were formed by condensation from vapor, not working in solution.

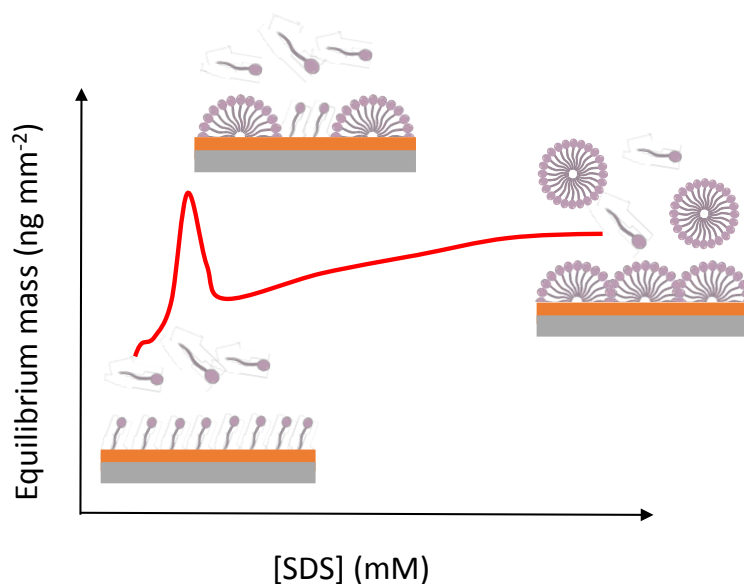


**Figure 32.** Adsorption model of SDS on C18 surface in different concentrations.

Regeneration and efficient usage of coenzymes are one of the most important challenges for large scale utilization of coenzyme-dependent enzymatic reactions. Accordingly, both DPI and SPR provided data about the immobilization of nicotinamide adenine dinucleotide dehydrogenase.<sup>192</sup> Both techniques were used to reliably monitor the regeneration and reactivity of that immobilized coenzyme in real-time. The conclusions achieved were of great importance for the rational design of multienzymatic reaction systems, principally in those cases in which immobilized multienzymes were involved.

Cross *et al.* studied found a correlation between the layer morphology of surfactants and their lipophilicity/hydrophilicity balance.<sup>193</sup> As a result, it was found that those with longer alkyl chains yielded thinner and denser layers at the hydrophobic solid/aqueous liquid interface. Moreover, an additional correlation was found between the degree of order achieved at sub-critical micelle concentrations and molecular fluidity.

Finally, Duan *et al.* described recently monitored the adsorption of sodium dodecyl sulfate (SDS) on a hydrophobic surface.<sup>194</sup> The authors observed that in dilute solution, the molecules adsorbed as isotropic layer, while in higher concentration hemimicelles were formed, inducing the anisotropy (Figure 32). On a dilute solution (SDS < 1 mM), the molecules regularly adsorbed on octadecyl carbon chain surface as a monolayer and the hydrophobic tail of the SDS molecule penetrates into and intercalates with the octadecyl carbon chain layer. However, hemimicelles aggregated on carbon surface when the SDS concentration exceeded 1 mM.

## **7. Future remarks**

Traditional analytical approaches have become insufficient to effectively address the growing number of challenges due to the current detection limits need in several fields. Recently, ever-increasing attention has been paid to hyphenated techniques as the principal instrument to deal with complex problems in biological, environmental and clinical samples. Two decades ago, Hirschfeld defined the term “hyphenation” as the on-line union of spectroscopic detectors and separation tools to exploit the advantages of both.<sup>195</sup> New developments are the combination of DPI with complementary technologies, so-called hyphenated DPI. In most cases, these technologies are coupled off-line and should be used serially; nevertheless both technologies share the sensor, which can be installed in the instrument as well as inspected with the other hyphenated techniques.

On the basis of the applications above described, DPI has proven to be a label-free technique that can be easily integrated with other complementary instrumentation in

the fields of functional proteomics and structural biophysics. This is the greatest challenge that this technology has to face. It should promote the joint use of DPI with AFM, dialysis methods, NR, SPR, QCM-D, NMR, FTIR, dynamic light scattering, etc. It is important to emphasize the advantages that each technique brings to the experiment. Advantages of combined techniques include the elimination of false positives, increased sensitivity of detection, and avoiding signal amplification steps. It allows important trends to be identified, recognizing new interrelations. Furthermore, complex processes can be monitored in a more complete manner, which leads to faster and better quantification and modeling. For example, the tandem DPI/QCM-D is able to identify the role of the hydration shell of proteins. That water plays an important role in the activity of proteins, so that after dehydration proteins cannot work. In spite of a huge work dealing with the hydration shell, this issue has not been clarified yet. Hence, this structural and mass tandem may allow the easy understanding of the influence of the hydration shell on the internal protein motions involved in its functioning.

In this line, the tandem DPI-mass spectrometry (DPI-MS) should increase in importance in the near future, as it may provide both quantitative and qualitative information. The basic idea is to follow up the characterization of interactions between proteins and surface-immobilized ligands by DPI with the determination of the identity of the bound proteins or peptides using MS. As such, MS utterly complements the DPI detection and reveals intrinsic protein structural modifications that go unregistered via the interferometric detection. This challenging tandem may have important applications in protein interaction discovery in proteomics and lipidomics, a recent research field with a brilliant future, and also in the characterization of protein modifications, which are critical for the interaction.

Various other combinations or potential for orthogonal measurements are also possible. One would be to measure the light lost from the waveguide, whether in terms of waveguide stimulated fluorescence or scatter. The former may be used for the characterization of fluorescent diagnostic assays of in a range of protein or lipid bilayer interaction experiments, and the latter could be utilized as a means of distinguishing scatter from absorption or for determining or imaging lateral structure in the film. It should also be possible to make electrically conducting waveguides,<sup>196</sup> which would enable simultaneous electrochemical and optical characterization, with a bewildering variety of potential uses such as studying the effect of surface change on adsorption and molecular orientation.

Future challenges in the development of silicon photonic biosensors may include achieving efficient lab-on-a-chip devices with on-chip detection. In this regard, present efforts are aimed to develop complete Si compatible and integrated devices; that is, interferometric systems with incorporated microfluidics and optoelectronics and a high level of sensitivity.<sup>197</sup> Accordingly, the coupling of lab-on-a-chip technology with DPI will provide an important advance for a huge number of new applications.

Another challenge that must be met in the future years is the incorporation of microfluidics to DPI to develop multiplexed arrays. Those platforms allow the advantageous and multiplexed delivery of many samples, or many probes to be anchored to the sensor. Their potential applications include diagnostics based on multiple biomarkers and the screening of potential therapeutic molecules in drug development. Moreover, bearing in mind the ability of DPI-MS tandem for the unambiguous

identification of the analyte after the binding event multiplexed sensing can even be performed for unknown analytes.

For the binding to the DPI surface to have maximum sensitivity and the signal to reflect the intrinsic kinetic and thermodynamic properties of the molecules under study, microfluidics appears to be the most powerful approach. Attractive features are excellent baseline stability, low sample consumption and the potential for relatively high mass transfer when high flow rates and thin channels are used. This technology can be very important when working with limited sample volumes, for better characterizing the thermodynamic binding parameters by permitting the binding progress to reach the steady state and be utilized to improve the sensitivity for analyte detection at low concentrations and in interfacing DPI with MS as outlined above.

Although lab-on-a-chip with the on-chip detection is still in its early beginnings, last advances led to the hope that the integration of optics-based biosensors and optofluidics could eventually be accomplished in the near-medium future. Most recent advances in technology are expected to give rise to automated and robust systems able to run minimizing operator skills.<sup>197</sup> Integrated optics technology is paving the way to truly portable lab-on-a-chip platforms with potential applications in food safety assessment, environmental pollution detection and fast diagnostics at the doctor office. Thanks to the intensive research effort performed at public and private institutions there are no doubts that lab-on-chip hand-held devices will be soon a reality in our future society.

## **8. Conclusions**

As can be seen from the multidisciplinary applications commented along this review, DPI is a label-free analytical technique that has provided important advancements in terms of quantifying and understanding recognition events in the design of new biosensors. Furthermore, DPI offers new insights into the macromolecular behavior in biological processes and has become a powerful technique to record real-time data of conformational dynamics in surface science and biophysics.

The key strengths of DPI are, in first place, the use of untagged reagents, which clearly simplifies the number of steps in the experimental procedure. Secondly, the short response time, which allows data updates at least every 20 ms, provides quantitative data on real-time changes in dimension, refractive index and density and thirdly the high sensitivity with resolution below 0.1 Å,  $10^{-7}$  refractive index units and 0.1 pg/mm<sup>2</sup>, respectively. For all these reasons, this technique offers a unique perspective on biochemistry, linking conformational changes to biochemical activity at a resolution usually attributed to 'big physics'. Additionally, DPI has three important features that offer a different approach in the investigation of biomolecules structure change, such as:

- Full structural characterization of every system in real-time (thickness, refractive index, surface concentration, density, area per molecule and volume fraction). This high level of quantitative characterization allows monitoring real-time actions of biomolecules which can be resolved as regard shifts in the layer's dynamic structure.
- Accurate measure of birefringence. When the birefringence is determined, it is possible to measure and follow changes in the supported anisotropic layer's

structure, which results in a better knowledge of the organization effects.

These studies have important applications in lipidomics.

- Kinetic analysis of the binding process. This means that structural alterations due to binding can be monitored in real-time, providing an incredible insight into the binding mechanism thanks to the technique performances.

It is interesting to point out the development of the multiple path length DPI (MPL-DPI),<sup>18</sup> which uses an arrangement similar to DPI. Nevertheless, MPL-DPI has the new capability of enabling *ex-situ* modifications of coatings after interruption of *in situ* experiments. That allows a more flexible approach in sample preparation which increases the amount of biotechnological applications.

Nevertheless, it is important to emphasize that DPI is emerging as a viable, rapid, label-free and highly sensitive technique that holds great potential in becoming a standard tool in functional biological studies and characterization for a wide variety of applications.

## **9. Acknowledgments**

We would like to thank Dr. Marcus Swann and Dr. Sergi Morais, with whom we have had many helpful discussions about DPI sensing and interferometry in general. We acknowledge the financial support from the Generalitat Valenciana (GVA-PROMETEO/2010/008), as well as the Spanish Ministry of Economy and Competitiveness and the European Regional Development Fund under award numbers CTQ/2010/15943 and CTQ2013-42914-R.

## 10. References

- (1) Binnig, G.; Rohrer, H. *Angew. Chem. Int. Ed.* **1987**, *26*, 606.
- (2) Eigler, D. M.; Schweizer, E. K. *Nature* **1990**, *344*, 524.
- (3) Clouthier, C. M.; Mironov, G. G.; Okhonin, V.; Berezovski, M. V.; Keillor, J. W. *Angew. Chem. Int. Ed.* **2012**, *51*, 12464.
- (4) Coan, K. E. D.; Swann, M. J.; Ottl, J. *Anal. Chem.* **2012**, *84*, 1586.
- (5) Cross, G. H.; Ren, Y.; Freeman, N. J. *J. Appl. Phys.* **1999**, *86*, 6483.
- (6) Freeman, N. J.; Cross, G. H. Chemical sensor. - Uses sensing and reference wave guides formed within substrate to detect polarised radiation. Patent WO9822807-A, May 28, 1998.
- (7) Cross, G. H.; Reeves, A. A.; Brand, S.; Popplewell, J. F.; Peel, L. L.; Swann, M. J.; Freeman, N. J. *Biosens. Bioelectron.* **2003**, *19*, 383.
- (8) Bunch, B. H.; Hellemans, A. *The History of Science and Technology*, Houghton Mifflin Company: New York, 2004.
- (9) Gestwicki, J.E.; Hsieh, H.V.; Pitner, J.B. *Anal. Chem.* **2001**, *73*, 5732.
- (10) Nellen, P.M.; Tiefenthaler, K.; Lukosz, W. *Sens. Actuat.* **1988**, *15*, 285.
- (11) Cross, G.H.; Ren, Y.; Swann M.J. *The Analyst* **2000**, *125*, 2173.
- (12) Cross, G. H. *Opt. Lett.* **2013**, *38*, 3057.
- (13) Cross, G. *Opt. Lett.* **2013**, *38*, 3057.
- (14) Cross, G. arXiv:1303.1390 [physics.optics] 6th March 2013.
- (15) Boudjemline, A.; Clarke, D. T.; Freeman, N. J.; Nicholson, J. M.; Jones, G. R. *J. Appl. Crystallogr.* **2008**, *41*, 523.
- (16) Xu, K.; Ouberai, M. M.; Welland, M. E. *Biomaterials* **2013**, *34*, 1461.
- (17) Coffey, P. D.; Swann, M. J.; Waigh, T. A.; Mu, Q.; Lu, J. R. *RSC Adv.* **2013**, *3*, 3316.
- (18) Coffey, P.; Swann, M. J.; Waigh, T.; Schedin, F.; Lu, J. *Opt. Express* **2009**, *17*, 10959.
- (19) Halthur, T.; Claessen, P.; Elofsson, U. *Langmuir* **2006**, *22*, 11065.
- (20) Mann, E. K.; Heinrich, L.; Schaaf, P. *Langmuir* **1997**, *13*, 4906.
- (21) Mashaghi, A.; Swann, M. J.; Popplewell, J. F.; Textor, M.; Reimhult, E. *Anal. Chem.* **2008**, *80*, 3666.
- (22) Horvath, R.; Ramsden, J. J. *Langmuir* **2007**, *23*, 9330.
- (23) Defeijter, J. A.; Benjamins, J.; Veer, F. A. *Biopolymers* **1978**, *17*, 1759.

- (24) Fernandez, D.; Le Brun, A.; Lee, T.; Bansal, P.; Aguilar, M.; James, M.; Separovic, F. *Eur. Biophys. J. Biophys.* **2013**, *42*, 47.
- (25) Homola, J. *Chem. Rev.* **2008**, *108*, 462.
- (26) Sonesson, A.; Callisen, T.; Brismar, H.; Elofsson, U. *Colloid. Surf. B* **2007**, *54*, 236.
- (27) Sonesson, A. W.; Callisen, T. H.; Brismar, H.; Elofsson, U. M. *Colloid. Surface B* **2007**, *54*, 236
- (28) Zwang, T.; Fletcher, W.; Lane, T.; Johal, M. *Langmuir* **2010**, *26*, 4598.
- (29) Kazarian, S. G.; Chan, K. L. A. *Analyst* **2013**, *138*, 1940.
- (30) Westwood, M.; Noel, T.; Parker, R. *Soft Matter* **2010**, *6*, 5502.
- (31) Lin, S.; Lee, C.; Lin, Y.; Lee, S.; Sheu, B.; Tsai, J.; Hsu, S. *Biosens. Bioelectron.* **2006**, *22*, 715.
- (32) Boudjemline, A.; Saridakis, E.; Swann, M. J.; Govada, L.; Mavridis, I. M.; Chayen, N. E. *Anal. Chem.* **2011**, *83*, 7881.
- (33) Protein Microarrays Ed. Mark Schena, Jones & Bartlett Pub: Sudbury, Massachusetts, 2004.
- (34) Yin, L.; Lu, M.; Wielunski L.; Song, W. ; Tan, J., Lu, Y. ; Jiang, W. *J. Opt.* **2012**, *14*, 085501.
- (35) Nakanishi, K.; Sakiyama, T.; Imamura, K. *J. Biosci. Bioeng.* **2001**, *91*, 233.
- (36) Wong, L. S.; Khan, F.; Micklefield, J. *Chem. Rev.* **2009**, *109*, 4025.
- (37) Cha, T. W.; Guo, A.; Zhu, X. Y. *Proteomics* **2005**, *5*, 416.
- (38) Awsiuk, K.; Budkowski, A.; Psarouli, A.; Petrou, P.; Bernasik, A.; Kakabakos, S.; Rysz, J.; Raptis, I. *Colloids Surf. B* **2013**, *110*, 217.
- (39) Morais, S.; Marco-Molés, R.; Puchades, R.; Maquieira, A. *Chem. Commun.* **2006**, 2368.
- (40) Lee, K. B.; Park, S. J.; Mirkin, C. A.; Smith, J. C.; Mrksich, M. *Science* **2002**, *295*, 1702.
- (41) Escorihuela, J.; Bañuls, M. J.; Puchades, R.; Maquieira, A. *Chem. Commun.* **2012**, *48*, 2116.
- (42) Jung, Y.; Lee, J. M.; Jung, H.; Chung, B. H. *Anal. Chem.* **2007**, *79*, 6534.
- (43) Mun, S.; Choi, S. J.. *Biosens. Bioelectron.* **2009**, *24*, 2522.
- (44) Fragoso, A.; Caballero, J.; Almirall, E.; Villalonga, R.; Cao, R. *Langmuir* **2002**, *18*, 5051.
- (45) Trilling, A. K.; Beekwilder, J.; Zuilhof, H. *Analyst* **2013**, *138*, 1619.
- (46) Frasconi, M.; Mazzei, F.; Ferri, T. *Anal. Bioanal. Chem.* **2010**, *398*, 1545.

- (47) Samanta, D.; Sarkar, A. *Chem. Soc. Rev.* **2011**, *40*, 2567.
- (48) Castello, J. G.; Toccafondo, V.; Escorihuela, J.; Bañuls, M. J.; Maquieira, A.; Garcia-Ruperez, J. *Opt. Lett.* **2012**, *37*, 3684.
- (49) Zhu, H.; Bilgin, M.; Bangham, R.; Hall, D.; Casamayor, A.; Bertone, P.; Lan, N.; Jansen, R.; Bidlingmaier, S.; Houfek, T.; Mitchell, T.; Miller, P.; Dean, R. A.; Gerstein, M.; Snyder, M. *Science* **2001**, *293*, 2101.
- (50) Rusmini, F.; Zhong, Z.; Feijen, J. *Biomacromolecules* **2007**, *8*, 1775.
- (51) Subramanian, A.; Irudayaraj, J.; Ryan, T. *Biosens. Bioelectron.* **2006**, *21*, 998.
- (52) Chen, Y. X.; Triola, G.; Waldmann, H. *Acc. Chem. Res.* **2011**, *44*, 762.
- (53) Jonkheijm, P.; Weinrich, D.; Koehn, M.; Engelkamp, H.; Christianen, P. C. M.; Kuhlmann, J.; Maan, J. C.; Nuesse, D.; Schroeder, H.; Wacker, R.; Breinbauer, R.; Niemeyer, C. M.; Waldmann, H. *Angew. Chem. Int. Ed.* **2008**, *47*, 4421.
- (54) Lutz, J. F. *Angew. Chem. Int. Ed.* **2008**, *47*, 2182.
- (55) Govindaraju, T.; Jonkheijm, P.; Gogolin, L.; Schroeder, H.; Becker, C. F. W.; Niemeyer, C. M.; Waldmann, H. *Chem. Commun.* **2008**, 3723.
- (56) Soellner, M. B.; Dickson, K. A.; Nilsson, B. L.; Raines, R. T. *J. Am. Chem. Soc.* **2003**, *125*, 11790.
- (57) de Araujo, A. D.; Palomo, J. M.; Cramer, J.; Kohn, M.; Schroeder, H.; Wacker, R.; Niemeyer, C.; Alexandrov, K.; Waldmann, H. *Angew. Chem. Int. Ed.* **2006**, *45*, 296.
- (58) Song, H.Y.; Hogley, J.; Su, X.; Zhou, X. *Plasmonics* **2014**, DOI: 10.1007/s11468-014-9680-9.
- (59) Luo, D.; Saltzman, W. M. *Nat. Biotechnol.* **2000**, *18*, 33.
- (60) Goodman, R. P.; Schaap, I. A. T.; Tardin, C. F.; Erben, C. M.; Berry, R. M.; Schmidt, C. F.; Turberfield, A. J. *Science* **2005**, *310*, 1661.
- (61) Johnston, A. P. R.; Zelikin, A. N.; Caruso, F. *Adv. Mater.* **2007**, *19*, 3727.
- (62) Bath, J.; Turberfield, A. J. *Nat. Nanotechnol.* **2007**, *2*, 275.
- (63) Campolongo, M. J.; Tan, S. J.; Xu, J.; Luo, D. *Adv. Drug Deliver. Rev.* **2010**, *62*, 606.
- (64) Jungmann, R.; Renner, S.; Simmel, F. C. *HFSP Journal* **2008**, *2*, 99.
- (65) Wang, F.; Liu, X.; Li, G.; Li, D.; Dong, S. *J. Mater. Chem.* **2009**, *19*, 286.
- (66) Liu, J. *Phys. Chem. Chem. Phys.* **2012**, *14*, 10485.
- (67) Bonanni, A.; Pividori, M. I.; del Valle, M. *Anal. Bioanal. Chem.* **2007**, *389*, 851.
- (68) Gajovic-Eichelmann, N.; Ehrentreich-Forster, E.; Bier, F. F. *Biosens. Bioelectron.* **2003**, *19*, 417.

- (69) Yan, F.; Sadik, O. A. *J. Am. Chem. Soc.* **2001**, *123*, 11335.
- (70) Bañuls, M. J.; Puchades, R.; Maquieira, A. *Anal. Chim. Acta* **2013**, *777*, 1.
- (71) Escorihuela, J.; Bañuls, M. J.; Grijalvo, S.; Eritja, R.; Puchades, R.; Maquieira, A. *Bioconjugate Chem.* **2014**, *25*, 618.
- (72) Escorihuela, J.; Bañuls, M. J.; Puchades, R.; Maquieira, A. *J. Mat. Chem. B*, **2014**, DOI: 10.1039/C4TB01108B.
- (73) Swann, M. J.; Peel, L. L.; Carrington, S.; Freeman, N. J. *Anal. Biochem.* **2004**, *329*, 190.
- (74) Shashilov, V. A.; Lednec, I. K. *Chem. Rev.* **2010**, *110*, 5692.
- (75) Lin, S.; Lee, C. K.; Wang, Y. M.; Huang, L. S.; Lin, Y. H.; Lee, S. Y.; Sheu, B. C.; Hsu, S. M. *Biosens. Bioelectron.* **2006**, *22*, 323.
- (76) Sheu, B. C.; Lin, Y. H.; Lin, C. C.; Lee, A. S.; Chang, W. C.; Wu, J. H.; Tsai, J. C.; Lin, S. *Biosens. Bioelectron.* **2010**, *26*, 822.
- (77) Thompsett, A.; Brown, D. R. *Biochim. Biophys. Acta, Proteins Proteomics* **2007**, *1774*, 920.
- (78) Karim, K.; Taylor, J. D.; Cullen, D. C.; Swann, M. J.; Freeman, N. J. *Anal. Chem.* **2007**, *79*, 3023.
- (79) Fresquet, M.; Jowitt, T. A.; Ylostalo, J.; Coffey, P. D.; Meadows, R. S.; Ala-Kokko, L.; Thornton, D. J.; Briggs, M. D. *J. Biol. Chem.* **2007**, *282*, 34634.
- (80) Gupta, S.; Modak, R.; Surolia, N.; Surolia, A. *Biochem. Bioph. Res. Co.* **2009**, *380*, 763.
- (81) Zwang, T. J., Patel, R., Johal, M. S., Selassie, C. R. *Langmuir* **2012**, *28*, 9616.
- (82) McPherson, A. *Crystallization of biological macromolecules*, Spring Harbor Laboratory Press: New York, 2001.
- (83) Vekilov, P. G.; Alexander, J. I. D. *Chem. Rev.* **2000**, *100*, 2061.
- (84) Boudjemline, A.; Clarke, D.T.; Freeman, N.J.; Nicholson, J.M.; Jones, G.R. *J. Appl. Crystallogr.* **2008**, *41*, 523.
- (85) Garcia-Caballero, A.; Gavira, J. A.; Pineda-Molina, E.; Chayen, N. E.; Govada, L.; Khurshid, S.; Saridakis, E.; Boudjemline, A.; Swann, M. J.; Stewart, P.; Briggs, R. A.; Kolek, S. A.; Oberthuer, D.; Dierks, K.; Betzel, C.; Santana, M.; Hobbs, J. R.; Thaw, P.; Savill, T. J.; Mesters, J. R.; Hilgenfeld, R.; Bonander, N.; Bill, R. M. *Crystal Growth & Design* **2011**, *11*, 2112.
- (86) Freeman, N. J.; Peel, L. L.; Swann, M. J.; Cross, G. H.; Reeves, A. A.; Brand, S.; Lu, J. R. *J. Phys. Condens. Mat.* **2004**, *16*, S2493.

- (87) Lu, J. R.; Swann, M. J.; Peel, L. L.; Freeman, N. J. *Langmuir* **2004**, *20*, 1827.
- (88) Sonesson, A.; Callisen, T.; Brismar, H.; Elofsson, U. *Colloid. Surface B* **2008**, *61*, 208.
- (89) Lundin, M.; Sandberg, T.; Caldwell, K. D.; Blomberg, E. *J. Colloid Interface Sci.* **2009**, *336*, 30.
- (90) Cowsill, B.; Coffey, P.; Yaseen, M.; Waigh, T.; Freeman, N. J.; Lu, J. *Soft Matter* **2011**, *7*, 7223.
- (91) Zhai, J.; Wooster, T. J.; Hoffmann, S. V.; Lee, T. H.; Augustin, M. A.; Aguilar, M. I. *Langmuir* **2011**, *27*, 9227
- (92) Zhai, J.; Hoffmann, S. V.; Day, L.; Lee, T. H.; Augustin, M. A.; Aguilar, M. I. *Langmuir* **2012**, *28*, 2357.
- (93) Krivosheeva, O.; Dedinaite, A.; Claesson, P. J. *Colloid Interface Sci.* **2012**, *379*, 107.
- (94) Krivosheeva, O.; Dedinaite, A.; Claesson, P. J. *Colloid Interface Sci.* **2013**, *408*, 82-86.
- (95) Krivosheeva, O.; Dedianite, A.; Linder, M. B.; Tilton, R. D.; Claesson, P. M. *Langmuir* **2013**, *29*, 2683.
- (96) Bingen, P.; Wang, G.; Steinmetz, N.; Rodahl, M.; Richter, R. *Anal. Chem.* **2008**, *80*, 8880.
- (97) Ash, A.; Ridout, M.; Parker, R.; Mackie, A.; Burnett, G.; Wilde, P. *Colloids Surf. B* **2013**, *102*, 546.
- (98) Ash, A.; Burnett, G. R.; Parker, R.; Ridout, M. J.; Rigby, N. M.; Wilde, P. J. *Colloids Surf. B* **2014**, *116*, 603-611.
- (99) Ouberai, M.M.; Xu, K.; Welland, M.E. *Biomaterials* **2014**, *35*, 6157.
- (100) Zhao, X.; Pan, F.; Cowsill, B.; Lu, J. *Langmuir* **2011**, *27*, 7654.
- (101) Moore, J.; Perez-Pardo, M.; Popplewell, J.; Spencer, S.; Ray, S.; Swann, M. J.; Shard, A.; Jones, W.; Hills, A.; Bracewell, D. *Biosens. Bioelectron.* **2011**, *26*, 2940
- (102) Gimenez-Romero, D.; Gonzalez-Martine, M. A.; Bañuls, M. J.; Monzo, I. S.; Puchades, R.; Maquieira, A. *J. Phys. Chem. B* **2012**, *116*, 5679.
- (103) Cowsill, B.; Waigh, T.; Eapen, S.; Davies, R.; Lu, J. *Soft Matter* **2012**, *8*, 9847.
- (104) Song, H.; Zhou, X.; Hobley, J.; Su, X. *Langmuir* **2012**, *28*, 997.
- (105) Platt, G.; Damin, F.; Swann, M. J.; Metton, I.; Skorski, G.; Cretich, M.; Chiari, M. *Biosens. Bioelectron.* **2014**, *52*, 82.
- (106) Jakob, U.; Kriwacki, R.; Uversky, V. N. *Chem. Rev.* **2014**, DOI: 10.1021/cr400459c.

- (107) Biehle, S.; Carrozzella, J.; Shukla, R.; Popplewell, J.; Swann, M.; Freeman, N.; Clark, J. *Biochim. Biophys. Acta, Mol. Basis Dis.* **2004**, *1689*, 244.
- (108) Thibault, G.; Houry, W. *J. Phys. Chem. B* **2012**, *116*, 6717.
- (109) Balhara, V.; Deshmukt, S. S.; Kálmán, L.; Kornblatt, J. A. *PlosONE* **2014**, *9*, DOI: 10.1371/journal.pone.0088395.
- (110) Daghestani, H.; Fernig, D.; Day, B. *Biosens. Bioelectron.* **2009**, *25*, 136.
- (111) Zhai, J.; Lee, T.; Small, D.; Aguilar, M. *Biochemistry* **2012**, *51*, 1070.
- (112) Gupta, S.; Babu, P.; Surolia, A. *Biomaterials* **2010**, *31*, 6809.
- (113) Rekas, A.; Jankova, L.; Thorn, D.; Cappai, R.; Carver, J. *FEBS J.* **2007**, *274*, 6290.
- (114) Ricard-Blum, S.; Peel, L.; Ruggiero, F.; Freeman, N. *Anal. Biochem.* **2006**, *352*, 252.
- (115) Popplewell, J.; Swann, M.; Ahmed, Y.; Turnbull, J.; Fernig, D. *ChemBiochem* **2009**, *10*, 1218.
- (116) Popplewell, J.; Swann, M.; Brown, G.; Lauder, B. *Methods Mol. Biol.* **2012**, *808*, 211.
- (117) Haupt, K. *Chem. Commun.* **2003**, 171.
- (118) Reddy, S.; Hawkins, D.; Phan, Q.; Stevenson, D.; Warriner, K. *Sens. Actuators, B* **2013**, *176*, 190.
- (119) Wu, G.; Jiang, X.; Zhou, L.; Yang, L.; Wang, Y.; Xia, G.; Chen, Z.; Duan, M. *J. Mol. Struct.* **2013**, *1045*, 47.
- (120) Wang, Y.; Jiang, X.; Zhou, L.; Yang, L.; Xia, G.; Chen, Z.; Duan, M. *Colloid Surface A* **2013**, *436*, 1159.
- (121) Sassolas, A.; Leca-Bouvier, B.; Blum, L. *Chem. Rev.* **2008**, *108*, 109.
- (122) Berney, H.; Oliver, K. *Biosens. Bioelectron.* **2005**, *21*, 618.
- (123) Lillis, B.; Manning, M.; Berney, H.; Hurley, E.; Mathewson, A.; Sheehan, M. *Biosens. Bioelectron.* **2006**, *21*, 1459.
- (124) Zhao, X.; Pan, F.; Coffey, P.; Lu, J. *Langmuir* **2008**, *24*, 13556.
- (125) Kato, N.; Lee, L.; Chandrawati, R.; Johnston, A.; Caruso, F. *J. Phys. Chem. C* **2009**, *113*, 21185.
- (126) Escorihuela, J.; Bañuls, M.; Castello, J.; Toccafondo, V.; Garcia-Ruperez, J.; Puchades, R.; Maquieira, A. *Anal. Bioanal. Chem.* **2012**, *404*, 2831.
- (127) Lopez-Paz, J. L.; Gonzalez-Martinez, M. A.; Escorihuela, J.; Bañuls, M. J.; Puchades, R.; Maquieira, A. *Sens. Actuators, B* **2014**, *192*, 221.
- (128) Huang, F.; Liang, H. *ACS Appl. Mater. Interfaces* **2013**, *5*, 5025.

- (129) Xu, P.; Huang, F.; Liang, H. *Biosens. Bioelectron.* **2013**, *41*, 505.
- (130) Huang, F.; Xu, P.; Liang, H. *Biosens. Bioelectron.* **2014**, *51*, 317.
- (131) Wang, J.; Xu, X.; Zhang, Z.; Yang, F.; Yang, X. *Anal. Chem.* **2009**, *81*, 4914.
- (132) Wang, J.; Coffey, P.; Swann, M.; Yang, F.; Lu, J.; Yang, X. *Anal. Chem.* **2010**, *82*, 5455.
- (133) Wang, Y.; Zheng, Y.; Yang, F.; Yang, X. *Chem. Commun.* **2012**, *48*, 2873.
- (134) Wang, Y.; Wang, J.; Yang, F.; Yang, X. *Anal. Chem.* **2012**, *84*, 924.
- (135) Ozalp, V. *Anal. Bioanal. Chem.* **2012**, *402*, 799.
- (136) Brown, H. A.; Marnett, L. J. *Chem. Rev.* **2011**, *111*, 5817.
- (137) Popplewell, J.; Freeman, N. J.; Carrington, S.; Ronan, G.; McDonnell, C.; Ford, R. *Biochem. Soc. T.* **2005**, *33*, 931.
- (138) Terry, C.; Popplewell, J.; Swann, M. J.; Freeman, N. J.; Fernig, D. *Biosens. Bioelectron.* **2006**, *22*, 627.
- (139) Popplewell, J.; Swann, M. J.; Freeman, N. J.; McDonnell, C.; Ford, R. *Biochim. Biophys. Acta, Biomembranes* **2007**, *1768*, 13.
- (140) Khan, T.; Grandin, H.; Mashaghi, A.; Textor, M.; Reimhult, E.; Reviakine, I. *Biointerphases* **2008**, *3*, FA90.
- (141) Mashaghi, A.; Swann, M. J.; Popplewell, J.; Textor, M.; Reimhult, E. *Anal. Chem.* **2008**, *80*, 5276.
- (142) Morley, S.; Cecchini, M.; Zhang, W.; Virgulti, A.; Noy, N.; Atkinson, J.; Manor, D. *J. Biol. Chem.* **2008**, *283*, 17797.
- (143) Sanghera, N.; Swann, M.; Ronan, G.; Pinheiro, T. *Biochim. Biophys. Acta, Biomembr.* **2009**, *1788*, 2245.
- (144) Yu, L.; Guo, L.; Ding, J.; Ho, B.; Feng, S.; Popplewell, J.; Swann, M. J.; Wohland, T. *Biochim. Biophys. Acta, Biomembr.* **2009**, *1788*, 333.
- (145) Nielsen, S.; Otzen, D. *J. Colloid Interface Sci.* **2010**, *345*, 248.
- (146) Lee, T.; Hall, K.; Swann, M.; Popplewell, J.; Unabia, S.; Park, Y.; Hahm, K.; Aguilar, M. *Biochim. Biophys. Acta, Biomembranes* **2010**, *1798*, 544.
- (147) Lee, T.; Heng, C.; Swann, M.; Gehman, J.; Separovic, F.; Aguilar, M. *Biochim. Biophys. Acta, Biomembranes* **2010**, *1798*, 1977.
- (148) Hosta-Rigau, L.; Stadler, B.; Yan, Y.; Nice, E.; Heath, J.; Albericio, F.; Caruso, F. *Adv. Funct. Mater.* **2010**, *20*, 59.
- (149) Lingwood, D.; Binnington, B.; Rog, T.; Vattulainen, I.; Grzybek, M.; Coskun, U.; Lingwood, C.; Simons, K. *Nat. Chem. Biol.* **2011**, *7*, 260.

- (150) Hirst, D.; Lee, T.; Swann, M. J.; Unabia, S.; Park, Y.; Hahm, K.; Aguilar, M. I *Eur. Biophys. J. Biophys.* **2011**, *40*, 503.
- (151) Baumann, M.; Swann, M.; Textor, M.; Reimhult, E. *Anal. Chem.* **2011**, *83*, 6267.
- (152) Ho, J.; Kuo, T.; Yu, L. *Anal. Chim. Acta* **2012**, *714*, 127.
- (153) Singh, S.; Kasetty, G.; Schmidtchen, A.; Malmsten, M. *Biochim. Biophys. Acta, Biomembr.* **2012**, *1818*, 2244.
- (154) Forbes, S.; McBain, A.; Felton-Smith, S.; Jowitt, T.; Birchenough, H.; Dobson, C. *Biomaterials* **2013**, *34*, 5453.
- (155) Karst, J.; Barker, R.; Devi, U.; Swann, M.; Davi, M.; Roser, S.; Ladant, D.; Chenal, A. *J. Biol. Chem.* **2012**, 287, 9200.
- (156) Fernandez, D.; Lee, T.; Sani, M.; Aguilar, M.; Separovic, F. *Biophys. J.* **2013**, *104*, 1495.
- (157) Singh, S.; Papareddy, P.; Kalle, M.; Schmidtchen, A.; Malmsten, M. *Biochim. Biophys. Acta, Biomembranes* **2013**, *1828*, 2709.
- (158) Singh, S.; Kalle, M.; Papareddy, P.; Schmidtchen, A.; Malmsten, M. *Biomacromolecules* **2013**, *14*, 1482.
- (159) Ouberai, M.; Wang, J.; Swann, M.; Galvagnion, C.; Guilliams, T.; Dobson, C.; Welland, M. *J. Biol. Chem.* **2013**, *288*, 20883.
- (160) Balhara, V.; Schmidt, R.; Gorr, S.; DeWolf, C. *Biochim. Biophys. Acta, Biomembranes* **2013**, *1828*, 2193.
- (161) Hirst, D.; Lee, T.; Swann, M. J.; Aguilar, M. I. *Anal. Chem.* **2013**, *85*, 9296.
- (162) Frost, R.; Jonsson, G.; Chakarov, D.; Svedhem, S.; Kasemo, B. *Nano Letters* **2012**, *12*, 3356.
- (163) Bijelic, G.; Shovsky, A.; Varga, I.; Makuska, R.; Claesson, P. *J. Colloid Interface Sci.* **2010**, *348*, 189.
- (164) Shovsky, A.; Bijelic, G.; Imre, V.; Makuska, R.; Claesson, P. *Langmuir* **2011**, *27*, 1044.
- (165) Shovsky, A.; Varga, I.; Makuska, R.; Claesson, P. *Langmuir* **2012**, *28*, 6618.
- (166) Shovsky, A.; Knohl, S.; Dedinaite, A.; Zhu, K.; Kjoniksen, A.; Nystrom, B.; Linse, P.; Claesson, P. *Langmuir* **2012**, *28*, 14028.
- (167) Edmondson, S.; Vo, C. D.; Armes, S. P.; Unali, G. F. *Macromolecules* **2007**, *40*, 5271.
- (168) Edmondson, S.; Vo, C.; Armes, S.; Unali, G.; Weir, M. *Langmuir* **2008**, *24*, 7208.
- (169) Lane, T.; Fletcher, W.; Gormally, M.; Johal, M. *Langmuir* **2008**, *24*, 10633.

- (170) Aulin, C.; Varga, I.; Claessont, P.; Wagberg, L.; Lindstrom, T. *Langmuir* **2008**, *24*, 2509.
- (171) Feldötö, Z.; Varga, I.; Blomberg, E. *Langmuir* **2010**, *26*, 17048.
- (172) Westwood, M.; Noel, T.; Parker, R. *Biomacromolecules* **2011**, *12*, 359.
- (173) Karabulut, E.; Wagberg, L. *Soft Matter* **2011**, *7*, 3467.
- (174) Marais, A.; Utsel, S.; Gustafsson, G.; Wågberg, L. *Carbohydr. Polym.* **2014**, *100*, 218.
- (175) Westwood, M.; Noel, T. R.; Parker, R. *Carbohydr. Polym.* **2013**, *94*, 137.
- (176) Westwood, M.; Roberts, D.; Parker, R. *Carbohydr. Polym.* **2011**, *84*, 960.
- (177) Lundin, M.; Solaqa, F.; Thormann, E.; Macakova, L.; Blomberg, E. *Langmuir* **2011**, *27*, 7537
- (178) Johnson, S.; Bronowska, A.; Chan, J.; Evans, D.; Davies, A. G.; Wälti, C. *Langmuir* **2012**, *28*, 6632.
- (179) Becker, A.; Zelikin, A.; Johnston, A.; Caruso, F. *Langmuir* **2009**, *25*, 14079.
- (180) Facca, S.; Cortez, C.; Mendoza-Palomares, C.; Messadeq, N.; Dierich, A.; Johnston, A.; Mainard, D.; Voegel, J.; Caruso, F.; Benkirane-Jessel, N. *Proc. Natl. Acad. Sci. U.S.A.* **2010**, *107*, 3406.
- (181) Lord, M. S.; Stenzel, M. H.; Simmons, A.; Milthorpe, B. K. *Biomaterials* **2006**, *27*, 1341.
- (182) Wang, Q.; Tam, K. *Langmuir* **2009**, *25*, 9898.
- (183) Varga, I.; Mezei, A.; Meszaros, R.; Claesson, P. *Soft Matter* **2011**, *7*, 10701.
- (184) Feldoto, Z.; Lundin, M.; Braesch-Andersen, S.; Blomberg, E. *J. Colloid Interface Sci.* **2011**, *354*, 31.
- (185) Hu, Y.; Jin, J.; Han, Y.; Yin, J.; Jiang, W.; Liang, H. *RSC Adv.* **2014**, *4*, 7716.
- (186) Myers, P.; Freeman, N. J.; Peel, L. L.; Swann, M. J. *LCGC Europe* **2008**, *21*, 68.
- (187) Volcke, C.; Gandhiraman, R.; Gubala, V.; Doyle, C.; Fonder, G.; Thiry, P.; Cafolla, A.; James, B.; Williams, D. *J. Colloid Interface Sci.* **2010**, *348*, 322.
- (188) Gubala, V.; Gandhiraman, R.; Volcke, C.; Doyle, C.; Coyle, C.; James, B.; Daniels, S.; Williams, D. *Analyst* **2010**, *135*, 1375.
- (189) Gandhiraman, R.; Gubala, V.; O'Mahony, C.; Cummins, T.; Raj, J.; Eltayeb, A.; Doyle, C.; James, B.; Daniels, S.; Williams, D. *Vacuum* **2012**, *86*, 547.
- (190) Carlborg, C.; Gylfason, K.; Kazmierczak, A.; Dortu, F.; Bañuls, M.J.; Maquieira, A.; Kresbach, G.; Sohlstrom, H.; Moh, T.; Vivien, L.; Popplewell, J.; Ronan, G.; Barrios, C.; Stemme, G.; van der Wijngaart, W. *Lab on a Chip* **2010**, *10*, 281.

- (191) Tan, O.; Cross, G. *Phys. Rev. E: Stat., Nonlinear, Soft Matter Phys.* **2009**, *79*.
- (192) Feng, X.; Gao, F.; Qin, P.; Ma, G.; Su, Z.; Ge, J.; Wang, P.; Zhang, S. *Anal. Chem.* **2013**, *85*, 2370.
- (193) Cross, G.H.; Reeves, D.; Brand, S.; Swann, M.J.; Peel, L.L.; Freeman, N.J.; Lu, J.R. *J. Phys. D: Appl. Phys.* **2004**, *37*, 74.
- (194) Duan, M.; Wang, H.; Fang, S.; Liang, Y. *J. Colloid Interf. Sci.* 2014, *417*, 285.
- (195) Wilson, I. D.; Brinkman, U. A. *J. Chromatogr. A* **2003**, *1000*, 325.
- (196) Brigitte, L.R.; Gez-Nagy, S.J.C. *Electroanalysis*, **2000**, *12*, 140.
- (197) Estevez, M.; Alvarez, M.; Lechuga, L. *Laser & Photonics Reviews* **2012**, *6*, 463.

## 11. Biographies



This is a group photo (from left to right): José Luis López-Paz, Rosa Puchades, Miguel Ángel González-Martínez, Jorge Escorihuela, Ángel Maquieira and David Gimenez-Romero

Jorge Escorihuela was born in 1979 in Castellón, Spain. He graduated in Chemistry in 2003 at Jaume I University of Castellón (Spain) and received a grant from the Spain Ministry of Education to pursue his PhD under the supervision of Santiago V. Luis and M. Isabel Burguete. He received his PhD in Green Chemistry in 2009. His doctoral research was focused on developing new chiral catalysts derived from amino acids and their application in catalytic asymmetric reactions. After completing his PhD,

he joined Prof. A. Maquieira and Prof. R. Puchades's group of the Institute of Molecular Recognition and Technological Development (IDM) at Polytechnic University of Valencia (UPV) as a research scientist in 2010. His current research interest is centered on the design of biosensors and DNA microarrays on silicon-based materials.

Miguel Angel González-Martínez graduated in Chemistry in 1990 from University of Valencia (UV, Spain). After two years in industry, he joined the Department of Chemistry of UPV and received his Ph.D. degree in Chemistry in 1998 under Professors A. Maquieira and R. Puchades. He continued performing post-doctoral research at the UPV and co-founded the Señal y Medida (SYM) research group from IDM belonging to UPV. He is Associate Professor of Analytical Chemistry at the UPV since 2002. His research is centered on automation in Analytical Chemistry, bioreagent immobilization and biosensing. He is also member of the Spanish Society of Analytical Chemistry.

José-Luis López-Paz received his B.S. and Ph.D. degrees in Analytical Chemistry from UV in 1991 and 1996, respectively. Following postdoctoral work in electrochemical detection of nucleic acids in Prof. Joseph Wang's group at New Mexico State University in 1998. He joined UPV in 2002 where he has been an Assistant Professor in the Department of Chemistry since 2005. After performing research on automation of

analytical methods he joined Prof A. Maquieira and R. Puchades's group at IDM in 2012. His current research is focused on optical sensors for biomolecular recognition.

Rosa Puchades was born in Valencia, on November 30, 1955. She received the M.Sc. and Ph.D. degrees in Chemistry from the University of Valencia in 1977 and 1982, respectively. Since 1979, she has been in the Department of Chemistry at UPV, where she is currently Professor of Analytical Chemistry and member of IDM. At present she is vice-rector for social responsibility and international cooperation at UPV. Her research interests involve screening methods the developing of bioMEMs and nanobiosensing systems applied in the life sciences, food, drug allergens, pathogens, pharmacogenetics, and organic pollutants. Dra. Puchades has co-authored around 200 papers published in international journals.

Ángel Maquieira is Full Professor of Analytical Chemistry at the Chemistry Department of UPV and member of IDM. His research interest topics include the developing of bioMEMs based on compact disc technology and nanobiosensing systems applied in the life sciences. Other study topics are related with biosensing and automation, support surfaces derivatization and functionalization, development of screening methodologies for food and drug allergens, pathogens, pharmacogenetics, and organic pollutants. He has coauthored more than 200 papers published in SCI journals.

David Gimenez-Romero, a native of Valencia, Spain, received his B.S. from UV in 1999 and his Ph.D. in Physical Chemistry in 2004. He spent three years as a postdoctoral researcher in the laboratory of Prof. Claude Gabrielli at the UMR 8235 CNRS-UPMC, where he used electrogravimetric methods to study the redox reactions of electroactive polymers. After completing his PhD, he joined Prof. Angel Maquieira and Prof. Rosa Puchades's group of IDM at UPV as a research scientist in 2012. He is currently a Doctor Assistant at UV and his research interest is centered on the study of protein conformational dynamics for the design of biosensors.

## Table of Contents graphic

